Queensland University of Technology
Brisbane Australia

This is the author's version of a work that was submitted/accepted for publication in the following source:

Siégel, Coralie, Schrank, Christoph, Bryan, Scott Edward, Beardsmore, Graeme, & Purdy, David John
(2014)
Heat-producing crust regulation of subsurface temperatures : a stochastic model re-evaluation of the geothermal potential in western Queensland, Australia.
Geothermics, *51*, pp. 182-200.

This file was downloaded from: https://eprints.qut.edu.au/63373/

© Copyright 2014 Elsevier

This is the author's version of a work that was accepted for publication in Geothermics. Changes resulting from the publishing process, such as peer review, editing, corrections, structural formatting, and other quality control mechanisms may not be reflected in this document. Changes may have been made to this work since it was submitted for publication. A definitive version was subsequently published in Geothermics, [VOL 51, (2014)] DOI: 10.1016/j.geothermics.2014.01.005

Notice: *Changes introduced as a result of publishing processes such as copy-editing and formatting may not be reflected in this document. For a definitive version of this work, please refer to the published source:*

https://doi.org/10.1016/j.geothermics.2014.01.005

*Manuscript
Click here to view linked References

Heat-producing crust regulation of subsurface temperatures: a stochastic model re-evaluation of the geothermal potential in southwestern Queensland, Australia.

C. Siégel [a,b,*], C. Schrank [a,c], S. E. Bryan [a,b], G. Beardsmore [d], D. Purdy [e]

[a] School of Earth, Environmental and Biological Sciences, Queensland University of Technology, Gardens Point Campus, 2 George Street, Brisbane, QLD 4001 Australia
[b] Queensland Geothermal Energy Centre of Excellence, The University of Queensland, St Lucia QLD 4072 Australia
[c] School of Earth and Environment, The University of Western Australia, 35 Stirling Highway, Crawley, WA 6009 Australia
[d] Hot Dry Rocks Pty Ltd, 36 Garden Street, South Yarra VIC 3141 Australia
[e] Geological Survey of Queensland, level 10, 119 Charlotte Street, Brisbane QLD 4000 Australia

* Corresponding author. E-mail address: c.siegel@qut.edu.au; coralie_s@hotmail.fr

Highlights

- A new temperature map of SW Queensland at 5 km depth has been produced, with 163 new heat flow data and temperature estimates at 5 km depth.
- 1D steady state conduction is a good predictor of deep temperature data on a regional scale.
- Effects of advective, convective or transient heat transfer are likely to be minor in this region.
- No evidence has been found of widespread high heat producing granites in SW Queensland
- A SW-NE trend of lower heat flow matches structural trends
- Areas of high crustal temperature in SW Queensland are associated with silicic crust relatively enriched in high heat producing elements between 5 and 40 km depth.

Abstract

A large subsurface, elevated temperature anomaly is well documented in Central Australia. High Heat Producing Granites (HHPGs) intersected by drilling at Innamincka are often assumed to be the dominant cause of the elevated subsurface temperatures, although their presence in other parts of the temperature anomaly has not been confirmed. Geological controls on the temperature anomaly remain poorly understood. Additionally, methods previously used to predict temperature at 5 km depth in this area are simplistic and possibly do not give an accurate representation of the true distribution and magnitude of the temperature anomaly. Here we re-evaluate the geological controls on geothermal potential in the Queensland part of the temperature anomaly using a stochastic thermal model. The results illustrate that the temperature distribution is most sensitive to the thermal conductivity structure of the top 5 km. Furthermore, the results indicate the presence of silicic crust enriched in heat producing elements between 5 and 40 km.

Keywords: geothermal; Australia; heat flow; thermal conductivity; stochastic modelling; inversion modelling

1. Introduction

Elevated geothermal gradients have long been recognised in the Great Artesian Basin (GAB) of central-eastern Australia (Polak and Horsfall, 1979, and references therein) (Fig. 1a). More recently, a regional map estimating the temperature at 5 km depth has been generated (Oztemp) (Somerville et al., 1994; Chopra and Holgate, 2005; Gerner and Holgate, 2010) as a basis for assessing the geothermal energy potential in Australia. The depth of 5 km was chosen as a cut-off for the economic extraction of geothermal energy (Chopra and Holgate, 2005). The map suggests the presence of a large (ca. 800,000 km^2) subsurface temperature anomaly (Oztemp anomaly) across central Australia and SW Queensland (Fig. 1b), with estimated temperatures greater than 235°C at 5 km depth, ca. 85°C (i.e., ca. 57%) higher than predicted from the average geothermal gradient for the upper continental crust (Somerville et al., 1994; Chopra and Holgate, 2005).

It is estimated that rocks in the Cooper Basin region, shallower than 5 km, hold ca. 7.8 million PJ available heat (Somerville et al., 1994; Bahadori et al., 2013) (Fig. 1b). Across the continent, Geoscience Australia has estimated that the crust shallower than 5 km contains thermal energy equivalent to 2,500,000 years worth of the total 2004-2005 energy consumption in Australia (Budd et al., 2006). Accordingly, geothermal exploration and development attracted multi-billion dollar work commitments from industry in Australia, with more than 400 geothermal tenements so far granted since 2001 (Dowd et al., 2011).

To date, generation of electricity from geothermal energy in central Australia and SW Queensland is limited to the 80 kWe (net) Birdsville geothermal plant (Bahadori et al., 2013) operating since 1992, a 20 kWe plant that operated on Mulka cattle station in South Australia (Lund and Boyd, 1999) for a short time from 1987, and a 1 MWe pilot plant commissioned by Geodynamics Ltd at Innamincka in May 2013. Recently, larger-scale projects have focused on Engineered Geothermal System (EGS) development at Innamincka, South Australia (Fig. 1b), where High Heat Producing Granites (HHPGs) are intersected at 3 to 5 km depth. In particular, heat flow studies indicate that the high temperatures observed at Innamincka are related to release of heat generated by radioactive decay within HHPGs at depth, below a thermally insulating sedimentary cover (Middleton, 1979; Gallagher, 1987; Beardsmore, 2004). It has thus been similarly predicted that anomalously high temperatures in SW Queensland (Fig. 1b) also result from subsurface HHPGs (e.g., Chopra and Holgate, 2005; Draper and D'Arcy, 2006). However, heat production values estimated from limited whole-rock chemical data for the few granites (Champion et al., 2007) intersected in petroleum wells to depths of ca. 3 km are substantially lower (1.6-4.2 μWm^{-3}) than those estimated for granites at Innamincka (9.7 μWm^{-3} for the Big Lake Suite Granite; Middleton, 1979).

Given the apparent absence of HHPGs (at < 5 km depth) beneath large tracts of the Oztemp anomaly, an important issue for geothermal energy assessment across this region is a critical appraisal of the quality of data upon which the temperature map was based. Important issues with the current Oztemp map are the use of: 1) linear extrapolations of borehole temperature measurements, as this may introduce errors because a conductive steady state temperature profile of continental crust must be non-linear in the presence of radiogenic material; 2) unreliable, shallow (e.g. < 500 m) temperature measurements extrapolated to 5 km depth, because shallow temperatures could be affected by past climatic variations (e.g., Bauer and Chapman, 1986); and 3) temperature extrapolations without considering material properties of the intersected lithologic formations, in particular, thermal conductivity and heat production of the rocks (e.g., Chapman, 1986).

The availability of heat flow data in Australia and across the GAB are limited with only two heat flow values reported for the Queensland part of the Oztemp anomaly (Gallagher, 1987; Goutorbe et al., 2008). Additional heat flow data have been measured at the continental scale using a linear relationship between the silica geothermometer and heat flow (Pirlo, 2002). However, the distribution of these values is heterogeneous across SW Queensland. Other heat flow determinations across the Oztemp anomaly are restricted to the

South Australian part of the Cooper Basin, (Beardsmore, 2004; Meixner et al., 2012). Consequently, the foundations of the Oztemp anomaly for SW Queensland are based on sparse surface heat flow data and currently, little evidence for buried high heat producing granitic rocks at depth.

The aim of this paper is to provide an improved understanding of the nature and origin of the thermal regime in SW Queensland as well as a re-assessment of the geothermal potential, both of which are crucial for the development of geothermal energy and to reduce exploration and development costs. This study provides 163 new heat flow data and temperature estimates at 5 km depth. A new temperature map at 5 km depth is presented to serve as a guide for more focused geothermal exploration studies. This map is based on stochastic thermal modelling, which permits a quantification of uncertainties of our estimates, and includes new thermal conductivity and heat production measurements on subsurface granitic rocks.

2. Geological Background

A large part of the Oztemp anomaly correlates with the extent of the Thomson Orogen; a poorly understood tectonic element in eastern Australia that separates Precambrian cratonic regions of central Australia from Phanerozoic fold belts developed along the eastern margin (Fig. 1c) (see recent reviews Fergusson and Henderson, 2013; Purdy et al., 2013). Through much of its extent, the Thomson Orogen is concealed by thick sedimentary cover (Fig. 1d) and as a result, tectonic interpretations are still debated. In particular, the nature of the underlying lower crust is disputed with some authors proposing it is oceanic crust (Harrington, 1974; Glen et al., 2013), whereas others have argued that it is Precambrian (Henderson, 1980; Finlayson, 1990) and silicic continental crust (O'Reilly and Griffin, 1990). Information on the nature of the Thomson Orogen basement derives from drilling (Fig. 1c), outcrops located outside the Oztemp anomaly in the Anakie Inlier and Charter Towers area (e.g., Fergusson and Henderson, 2013; Purdy et al., 2013), and from geophysical methods such as gravity, magnetic and deep crustal seismic transects (Fig. 2). Across the Oztemp anomaly, ca. 780 drill holes intersect Thomson orogen-related rocks at 1 to 4 km depth (Brown et al., 2012) (Fig. 1c). Information from these holes suggests that the uppermost stuctural levels are primarily composed of low-grade metasedimentary rocks, lesser granitic intrusions (ca. 52 intersections) and volcanic rocks (ca. 15 intersections). The thickness of the lower crust is revealed by deep crustal seismic transects that indicate the Moho is located at ca. 40 km depth (Finlayson et al., 1990). Along the Brisbane-Eromanga transect (a 1100 km long E-W geophysical transect in southern Queensland; Fig. 2), the crust is considered to be more silicic to the west based on low magnetization and low Bouguer anomalies (O'Reilly and Griffin, 1990).

Additional information on the nature of the crust derives from extrapolation of xenolith studies in Eastern Australia (O'Reilly and Griffin, 1990) (Fig. 2) and an exposed crustal profile in the Arunta and Musgrave Inliers of central Australia (Sandiford et al., 2001). Within this exposed crustal profile, the abundance of high heat producing rocks varies with depth. Importantly, the crust between 6 and 10 km depth is highly enriched in heat producing elements. For example, the Teapot Granite Complex has an estimated heat generation of 5.9 +/-1.7 μWm^{-3} (Sandiford et al., 2001).

The lack of recent magmatic activity and seismicity across the Oztemp anomaly suggests that the area is tectonically stable. The youngest known intrusive rocks are the Permo-Carboniferous Big Lake Suite granodiorites at Innamincka (Gatehouse et al., 1995; Marshall, 2013). Additionally, only 23 earthquakes were detected in the Queensland part of the Oztemp anomaly during the last century and of those, only two are of magnitude > 4 (GA Earthquake Database http://www.ga.gov.au/earthquakes/searchQuake.do).

Deep HHPGs serve as a potential reservoir for EGS development. Consequently, if appropriate drilling targets are to be identified, it is crucial to understand the distribution and character of the subsurface granitic rocks. Across the Queensland part of the Oztemp anomaly, the 52 granitic intrusions intersected in drill holes are distributed heterogeneously (Fig. 1c) and vary in composition from syenogranite to monzogranite, from I to S-type, and from fresh (LOL Stormhill 1) to strongly altered (DIO Wolgolla 1) (Murray, 1994). Limited data indicate low heat production (< 5 μWm^{-3}) (Champion et al., 2007) and crystallisation ages from 400 to 860 Ma, with two clusters at ca. 420 to 430 Ma SE of Innamincka and ca. 470 Ma near Longreach (Murray, 1994 and references therein; Draper, 2006).

In contrast, the adjacent Big Lake Suite intrusions that are the focus of EGS development in Australia have emplacement ages of ca. 310 to 330 Ma (Gatehouse et al., 1995; Marshall, 2013) and higher heat production values (ca. 7 to 9.7 μWm^{-3}) (Middleton, 1979). East of the Oztemp anomaly, in the Roma Shelf area (north and south of Roma, Figs. 1b and 1c) intrusive rocks are extensive below the sedimentary cover. These are known as the

‘Roma Granites’ and have emplacement ages ranging from 320 to 350 Ma (Murray, 1994) but lack the geochemical data needed to calculate heat production values.

High thermal resistance due to thick and/or low conductive sedimentary blanketing can effectively trap heat (e.g., thick formations enriched in low conductive materials like coal and shale) (Mildren and Sandiford, 1995), and is thus another key parameter for EGS exploration. In central western Queensland, episodes of repeated basin subsidence and sediment accumulation have occurred since the early Paleozoic, resulting in a series of stacked basins (Fig. 3) and sediment thicknesses up to 4 km (Fig. 1d) (e.g., west of Bayrick and beneath the Cooper Basin). Major basin systems include: 1) the Devonian Adavale Basin, Warrabin Trough and Barrolka Trough; 2) the Late Devonian-Early Carboniferous Drummond Basin; 3) the mid Carboniferous to mid Triassic Galilee Basin; 4) the early Permian to mid Triassic Cooper Basin; and 5) the very extensive Jurassic to Cretaceous Eromanga and Surat basins, components of the Great Australian Superbasin (Cook et al., 2013).

3. Methodology

3.1. Approach and Limits

To re-evaluate the geothermal potential in western Queensland, heat transfer mechanisms across the intersected formations must be evaluated. Most geothermal studies assessing surface heat flow assume dominantly vertical conduction (Ricard and Chanu, 2013 and references therein), and in this study, we have adopted this assumption. However, if thick, permeable sedimentary sequences are present, advection and convection can affect heat transfer in the continental crust significantly, as shown for example, in the Perth Basin, WA (Sheldon et al., 2012; Schilling et al., 2013). Previous studies have used a wide range of methods to estimate heat flow, depending on the quality, quantity and type of data available. These include methods based on thermal conductivity and temperature gradient measurements (for a review, see Beardsmore and Cull, 2001). While the most direct methods to determine the surface heat flow are based on the product of thermal conductivity and temperature gradient, other methods such as inversion methods, assume a set of thermal conductivity characteristics and determine a heat flow value to minimise error between the modelled and observed temperature profiles (Matthews, 2009; Kirkby and Gerner, 2010; Korsch et al., 2011). In this study we use this latter approach.

We used 163 wells in the study area (ca. 1300 km x 850 km; Fig.1d), in which temperature, thermal conductivity and heat production data were recorded (refer to Section 3.2 for details). For these wells a conductive temperature profile was calculated to best fit the observed temperature measurements, using a one-dimensional inversion model. Subsequently, the temperature was extrapolated to a depth of 5 km as detailed in Appendix A. Table 1 provides the list of parameters used in the thermal modelling.

Wells were selected according to the following criteria: 1) geographical location to provide sufficient spatial coverage for data interpolation maps; and 2) quantity and quality of available information; lithologic descriptions and reliable temperature measurements (e.g., Horner plots and/or including drill stem tests).

3.2. Input parameters

3.2.1. Stratigraphy

The stratigraphy of the basins must be taken into account for determining the material properties of intersected sedimentary formations. The stratigraphy for each well was established using the most recent stratigraphic constraints (Cook et al., 2013; Fergusson and Henderson, 2013; Withnall and Hutton, 2013), information from well completion reports and an unpublished compiled database from the Geological Survey of Queensland. The general stratigraphy for each basin is reported in Table 2. Additional details for each well are available in Supplement 1 (also publically available at http://eprints.qut.edu.au/63373/).

3.2.2. Thermal conductivities

Surface heat flow is a function of thermal conductivity (Fourier, 1822). Thermal conductivity of a rock depends on several physical parameters such as lithology, porosity, pore fluids, temperature, the nature and proportion of its constituents and its microstructure (for a review, see Clauser and Huenges, 1995). The general range of thermal conductivities for geomaterials covers about one order of magnitude, with values from ca. 0.2 $Wm^{-1}K^{-1}$ for coal, to ca. 5.5 $Wm^{-1}K^{-1}$ for dolomite and quartzite (Beardsmore and Cull, 2001). Porosity can have a strong control on the thermal conductivity of a sedimentary formation, with values ranging from ca. 2.3 to 6 $Wm^{-1}K^{-1}$ in sandstone, for > 25% and 0% porosity, respectively (Gallagher, 1987). The effect of temperature on thermal conductivity is relevant in areas where the temperature varies significantly (for most crystalline rocks, a decrease of ca. 10 to 50% occurs from 0°C to about 300°C, Seipold 1998). Lithology, porosity and temperature should therefore be taken into account when estimating thermal conductivity for thermal modelling.

To limit the uncertainty of thermal conductivity for a particular formation, thermal conductivity measurements of representative samples are desirable. In general, thermal conductivity measurements are preferred within single wells to determine the surface heat flow. Samples are selected for different lithologies within the section and used in association with knowledge of the relative percentage of those lithologies. However, the selection of a representative sample can be difficult due to large vertical lithological variations within some formations, and because not all lithologies within a formation have always been sampled (Meixner et al., 2012). A review of publically available data for the studied area indicates a generally large standard deviation for the measured thermal conductivity (Table 2). For example, among 25 measured average thermal conductivity values, 9 have a relative standard deviation > 30%, with a maximum of 64 % for the Early Permian Epsilon Formation (Cooper Basin). Additionally, thermal conductivity measurements are not available for all sedimentary formations encountered in SW Queensland. Available thermal conductivity measurements are concentrated for formations within the Eromanga and Cooper basins, but data are sparse for the Surat basin, and none have been reported from the Galilee, Drummond, Adavale and Georgina basins. The available measurements are thus not necessarily representative (Meixner et al., 2012).

Our study is at a regional scale and therefore it is desirable to use representative thermal conductivities for each formation. Thermal conductivities were estimated for all formations encountered in this study, using an average thermal conductivity for a particular lithology, correcting for porosity and saturation when information is available and also correcting for temperature. Methods to estimate the average thermal conductivity of a formation include the use of: 1) geophysical logs (Goutorbe et al., 2006); 2) a compaction model based on the concept of loss of porosity with depth (Yorath and Hyndman, 1983); and 3) lithologic descriptions and applying corrections for temperature, porosity and the nature of the saturants (Beardsmore, 2004). In this study, we used the approach of Beardsmore (2004). To account for lithologic variations within a sedimentary formation, detailed lithologic descriptions (based on reports of ditch cutting and core compositions) for three wells were used to estimate an arithmetic mean thermal conductivity (i.e., an upper-bound estimate, e.g., Maze and Wagner 2009) and a standard deviation. For formations where lithologic proportions where reported in comparative terms, we used the following to convert to percentage: “dominant” = 80%; “minor” = 20%; “occasional” or “grading” or “contains” = 10%; “very minor” = 5%, “rare” or “traces” = 1% and “interbedded” = equal proportions (Beardsmore, 2004). The effect of porosity and volumetric percentage of the nature of the saturants (oil, gas, of water) on the bulk thermal conductivity, when available, were corrected using the geometric mean model (Eq. (1); Gallagher, 1987).

$K_b = (K_m)^{1-\emptyset} \, (K_s)^{\emptyset}$ Eq. (1),

where K_b is the bulk thermal conductivity, K_m the matrix conductivity and $\emptyset$ is the porosity. The matrix conductivities were taken from (Beardsmore 2001). In cases where no porosity information was available, the thermal conductivity was estimated using average lithologic values (Beardsmore and Cull, 2001). Where the nature of the saturants was unknown, the formations were assumed to be 100% water saturated.

Once a mean thermal conductivity was estimated for a formation, it was subsequently corrected for temperature. Several empirical relationships have been proposed for the temperature dependence of thermal conductivity (for a review, see Clauser and Huenges, 1995). The empirical relationship proposed by Birch and Clark (1940) was successfully tested by Sass et al. (1992) on an independent dataset. This correction was adopted here:

$K(T) = \frac{K(0)}{1.007 + T\left(0.0036 - \frac{0.0072}{K(0)}\right)}$ Eq. (2),

where: $K(0) = K(25)\left[1.007 + 25\left(0.0037 - \frac{0.0074}{K(25)}\right)\right]$.

The temperature (T) for the mean depth of the sedimentary formation interval was determined by linear interpolation of all reliable temperature measurements from each well. Further details on the estimation of thermal conductivities are available in Supplements 1 and 2 (also publically available at http://eprints.qut.edu.au/63373/).

Eight new thermal conductivity measurements on granitic rock sampled from drill cores were performed for this study and are reported in Table 3 and discussed in Section 4.2. For each sample, two or three thermal conductivity measurements were undertaken at room temperature (25ºC) along the core axis of each sample using a steady state divided bar apparatus. The instrument was calibrated for the range of thermal conductivity 0.4-12 $Wm^{-1}K^{-1}$. Three cylindrical specimens (each specimen 1/3 to 1/2 its diameter in thickness) of each granitic sample were cut, ground flat and polished to a standardized flatness and grit (except for the TEP Jandowae West 1 sample, from which only two specimens could be prepared). The specimens were evacuated under vacuum for a minimum of three hours, then submerged in water and subsequently returned to atmospheric pressure. Water saturation continued under atmospheric pressure for a minimum of sixteen hours prior to the conductivity measurement. Thermal conductivity measurements reported in Table 3 correspond to the harmonic mean (i.e., the lower-bound estimate) and standard deviation of the analyses performed on the 2-3 measurements. Granitic intrusions in the study area rarely display the same degree of vertical lithologic variation as sedimentary units. They are typically more homogeneous with depth, and thus thermal conductivity measurements of the granitic bodies are considered regionally representative.

3.2.3. Temperature

Fourier's first law (1822) shows that heat flow depends as much on the geothermal gradient as thermal conductivity. Temperatures recorded by the petroleum industry are usually of two types: Bottom Hole Temperature measurements (BHTs) acquired near the bottom of the hole during geophysical logging, and temperature of the reservoir fluids measured during Drill Stem Tests (DST).

It is well recognised that BHTs are recorded under transient thermal conditions. BHTs are primarily affected by the cooling effect of the circulating drilling fluids and thus generally underestimate the true formation temperature by ca. 10°C (Goutorbe et al., 2007). To estimate the true formation temperature, a wide-range of corrections have been proposed (for review, see Goutorbe et al., 2007). The Horner correction method is the most utilised technique (Kutasov and Eppelbaum, 2009 and references therein) and has been adopted here to correct BHT measurements in the study area. The Horner correction method requires the use of at least two, but ideally three or more, BHT measurements at similar depth and different shut-in times, i.e., at a different time after the circulation of the fluids. A summary of this method is available from Chapman et al. (1984).

DST temperatures are generally more reliable, less variable and require no specific correction (Förster et al., 1997). DSTs record the temperature of the fluids extracted from the walls of the borehole. They are considered to be at equilibrium with the surrounding rocks and represent true formation temperatures (Förster et al., 1997).

The available subsurface temperature measurements in SW Queensland have been compiled into the single Oztemp dataset (Holgate and Gerner, 2011). Overall, the spatial distribution of the data is not homogeneous and the quality of individual data points is not always high. The number of temperature measurements within individual boreholes is generally very limited with only 383 wells amongst 5442 wells in Australia having more than two reliable temperature measurements at depth (>1 km). Additionally, the quality of the data is yet to be fully evaluated (Meixner et al., 2012). We compared the Oztemp dataset with individual well completion reports and identified discrepancies in temperature data (e.g., measured temperature and/or depth of measured temperature, or data not recorded) for ten wells among the 163 wells studied (Table 5). Such errors can be significant, and for CON Lynwood 1 (25°35’25’’E and 143°31’36’’E), a difference of 31°C/km in the calculated average thermal gradient was discovered (70°C/km using Oztemp data versus 39°C/km from data in the well completion report). To ensure data quality, each temperature datum used in this study was systematically cross-checked against the well completion reports. Generally, several temperature measurements are available at different depths and are used to predict the ‘best-fit’ temperature profile. In total, for the 163 wells, 464 temperature measurements were used for thermal modelling. These are listed in Supplement 2 (also publically available at http://eprints.qut.edu.au/63373/). Amongst the 163 wells, 75 wells have both DST and Horner-corrected data, 33 wells have DST, 50 have Horner data, 4 are uncorrected BHT and 1 is unknown.

The mean surface temperature in the area is considered to be homogeneous at 25°C, consistent with a previous study of the thermal state of the Cooper Basin (Beardsmore, 2004). The impact of variation in mean surface temperature on the predicted temperature at 5 km depth was tested with the stochastic approach. The estimated temperature at 5 km depth only varied by 1°C for a 13°C change at the surface.

3.2.4. Heat Production

Heat production rates for basement granites was estimated from the concentration of U (C_U), Th (C_{Th}) and K (C_{K2O}) and a density, ρ, of 2.65 g/cm^3 using the equation of Rybach and Buntebarth (1981):

$$A = 10^{-5}\, \rho \left(9.52\, C_U + 2.56\, C_{Th} + 3.48\, C_{K_2O}\right) \text{ Eq. (3).}$$

Heat production of each sedimentary formation was considered constant with a value of 1.87 µWm^{-3}, based on average U, Th and K concentrations from Kamber et al. (2005) (Table 4). This value was determined for the volcanogenic Rolling Downs Group of the GAB and may only be applicable to this particular rock suite. However, previous studies have also used values of this order for sedimentary rocks. For example, in Queensland a value of 1 µWm^{-3} was used for sedimentary rocks in the Millungera and Eromanga basin (Korsch et al., 2011), and 1.2 and 1.4 µWm^{-3} for the Eromanga and Cooper basins, respectively (Meixner et al., 2012). The adopted value of 1.87 μWm^{-3} represents an upper-bound estimate and thus leads to a more conservative estimate of heat flow contributed by radiogenic granitic rock. Concentrations of U, Th and K for ten intersected granitic rocks are available from Champion et al. (2007) and the late BW Chappell (unpublished data). They indicate heat production values are low, ranging from 1.8 to 4.2 μWm^{-3}. Our new measurements (Table 4) on an additional 8 samples confirm a low to medium heat production capacity of intersected granitic rocks in SW Queensland.

Where available, we applied measured values for granite heat production. Otherwise a heat production value of 2.5 μWm^{-3} was used, as estimated by Meixner et al. (2012) using available whole-rock chemistry of Australian granites (Champion et al., 2007). Heat production for other types of basement rocks was considered to be 1.7 μWm^{-3}(Meixner et al., 2012), using global upper crustal averages of U, Th and K concentrations (Rudnick and Gao, 2003).

3.3. Stochastic Approach

Measured or estimated values of thermal conductivity, temperature and heat production are affected by a wide range of parameters, the poor knowledge of which limits the capability of determining accurate values of heat flow. Moreover, insufficient sampling across the regional study area imposes a fundamental uncertainty of material properties and temperature data. It is therefore important to consider the impact of variance in these parameters on the uncertainty of the calculated heat flow and extrapolated temperature at 5 km depth (Fig. 4). Previous geothermal studies have used a stochastic or Monte-Carlo approach to characterise the uncertainty of the calculated output (e.g., Srivastava and Singh, 1999; Ferrero and Gallagher, 2002; Srivastava, 2005; Meixner et al., 2012). The value of such approaches has been pointed out by Korsch et al. (2011) who modelled heat flow in the Millungera basin using nine different scenarios. The calculated heat flow varied by up to 20 mWm^{-2}. This large uncertainty associated with the estimation of thermal conductivity and the type of temperature correction justifies the use of a Monte-Carlo approach, which has been adopted here.

We consider the following parameters as the main sources for the uncertainty in our temperature estimates: thermal conductivity, volumetric heat production and temperature measurements. These parameters were perturbed in our models according to a specific probability density function. For each well, 1000 realisations with randomly perturbed input parameters were calculated. For temperature and heat production, a normal distribution was employed with a standard deviation of 1.5ºC and 0.5 μWm^{-3}, respectively (Fig. 4). The temperature and heat production estimates obtained from the wells and the laboratory were used as means (Supplement 2; also publically available at http://eprints.qut.edu.au/63373/). The probability distribution used for the thermal conductivity is assumed to be lognormal as suggested by the compilation of existing thermal conductivity data (Meixner et al., 2012). The mean and standard deviation for the lognormal distribution of thermal conductivities are those that have been estimated and reported in Table 2. For the global model, all three parameters (heat production, thermal conductivity and temperature) are perturbed.

The uncertainty of which of the three parameters or their combinations has the largest effect on heat flow estimates was also examined. To this end, a well with particularly well-constrained temperature measurements (DIO Macadama 1) was chosen. Simulations of all 8 possible permutations of keeping none, one, or more parameters fixed while perturbing the others were run. The results are presented and discussed in Section 4.4.

3.4. Interpolation techniques

For visualisation of the results on a map (Figs. 6, 7 and 8a) we used Inverse Distance Weighting (IDW) for interpolation. More sophisticated interpolation methods such as Kriging require that the data are normally distributed (which is not the case here), and are thus not applicable. However, it must be noted that interpolations do not represent geostatistically thorough predictions. The data used for interpolation can be found in Supplement 3 (also publically available at http://eprints.qut.edu.au/63373/).

4. Results

The results of the stochastic thermal model, i.e., temperature and heat flow estimates at 5 km depth can be found in Supplement 3 (also publically available at http://eprints.qut.edu.au/63373/).

4.1. Heat production

The intrusive rocks sampled in this study range from leucocratic monzogranite to tonalite and monzodiorite and include both S-type and I-type compositions (Table 3). Heat production values estimated for these rocks range from 0.75 to 4.87 μWm^{-3}. Granite in TEP Jandowae West 1, located close to Brisbane and well east of the temperature anomaly has the lowest heat production value while granite intersected in PGA Bradley 1, located outside the Oztemp anomaly to the west has the highest value. Most granitic rocks analysed here have heat production values greater than the upper continental crust. However, this enrichment is significantly lower than that observed for the Big Lake Suite granodiorite (Table 4) and confirms the lack of HHPG intersected in drill cores across the Oztemp anomaly area.

4.2. Thermal conductivity measurements

New thermal conductivity measurements on eight granitic samples range from 2.5 to 3.7 $Wm^{-1}K^{-1}$ and are within the range of published values for similar granite lithologies (Zoth and Haenel, 1988). Granitic rocks generally exhibit low porosities (Clauser and Huenges, 1995); therefore, the variation of thermal conductivity mainly depends on mineralogy. The low bulk thermal conductivity (2.5 $Wm^{-1}K^{-1}$) of this monzodiorite intrusion (TEP Jandowae West 1) is explained by the high abundance of plagioclase (45 vol%), a low conductivity phase (ca. 2.1 $Wm^{-1}K^{-1}$), and the low abundance of highly conductive quartz (10 vol%; > 6 $Wm^{-1}K^{-1}$) (Table 3) (Clauser and Huenges, 1995).

4.3. Stochastic modelling: the effect of input parameter on uncertainty

Eight simulations were undertaken to examine the influence of input parameters on the calculated heat flow and temperature at 5 km depth (Fig. 5). We picked DIO Macadama 1 as an example because it provides the best temperature constraints. The eight simulations represent all possible permutations of perturbed versus fixed input parameters. Simulations 1, 4, 6 and 8 all include thermal conductivity as a variable parameter. These simulations display a wide range of uncertainty (up to 25 mWm^{-2} and 20ºC) suggesting that thermal conductivity has the strongest influence on estimated heat flow and temperature, in agreement with Meixner et al. (2012). Simulations 2, 3, 5 and 7, for which thermal conductivity is fixed, exhibit small variability of less than 5 mWm^{-2} and 5ºC at 5 km depth, and a higher median than simulations 1,4, 6 and 8. The differences in median heat flow and median temperature between those two groups of simulations are up to 10-15 mWm^{-2} and 5ºC, respectively. Thermal conductivity is thus a crucial parameter that should be carefully constrained to minimise the uncertainty of heat flow and deep temperature determination.

4.4. Stochastic modelling: the effect of the perturbation distribution

The stochastic model discussed in Section 4.3 suggests that the predicted temperatures and heat flows at 5 km depth vary widely depending on the thermal conductivity data (Fig. 5). The question arises as to which degree the choice of the perturbation distribution for thermal conductivity affects the model predictions? In the simulations described below, a lognormal distribution based on the statistical evaluation of existing material data for the region (Meixner et al., 2012) was employed. To obtain a conservative estimate of the impact of the choice of perturbation function, a simulation in which a uniform probability distribution with bounds of 0.1 to 5 $Wm^{-1}K^{-1}$ was used. This is equivalent to assuming that no a-priori knowledge of thermal conductivity exists except for lower and upper bounds. 1000 model realisations were run keeping temperature and heat production fixed because these two parameters have a negligible effect on the results. The results are illustrated in Figures 6g and 6h. They indicate an uncertainty of ca. ±20% for temperature estimation at 5 km depth and a significantly underestimated heat flow (ca. -40%) using a uniform distribution of thermal conductivity and fixing the other parameters. However, this result is unlikely to represent the natural case because material properties with lower and upper bounds thermal conductivity values are rare. Our a-priori knowledge of thermal conductivities is therefore useful and must be considered in any quantitative heat flow determinations. It is also interesting to note that the strong SW-NE trend of lower heat flow is reproduced (see Fig. 6h).

4.5. New temperature and heat flow map at 5 km depth

The new predicted temperature map for 5 km depth (Fig.6a) has significant differences compared to the Oztemp temperature map of Gerner and Holgate (2010). The regional extent of the Oztemp anomaly is much smaller with a prominent SW-NE trend of elevated temperatures (200-250°C) (Fig. 6a). Only scattered anomalous temperatures are now predicted north of the Roma Shelf and in the Georgina Basin.

A lower heat flow zone (Fig. 6b) with values ranging from 80 to 100 mWm^{-2} is observed between domains with heat flow > 100 mWm^{-2} and is oriented along a SW-NE trend. This trend parallels, and is adjacent to, the high temperature trend described above. While the data points are clustered along this trend, the contouring SW-NE pattern persists when interpolating more evenly distributed data points over a smaller area (25º20’0’’E - 27º10’0’’E and 141º2’0’’E - 144º2’0’’E), Therefore the contouring trends are not directly affected by the distribution of the data points.

First quartile and third quartile maps, which correspond to 25% and 75% cumulative probability, respectively, (Figs 6c to 6f) are very similar in terms of spatial distribution, confirming the SW-NE trend. The quartile maps provide an upper and lower bound for the estimated temperature and heat flow at 5 km depth, indicating an uncertainty due to material properties of ca. ±10% for both parameters. Globally, areas with elevated heat flow at 5 km depth are also characterised by high temperature at 5 km depth. An exception occurs towards the Galilee Basin (Figs. 3, 6a and 6b) where heat flow is high (ca. 100 mWm^{-2}) and temperatures generally lower (three temperature measurements below 170°C). Such differences may result from changes in the thermal conductivity of the sedimentary cover, with higher thermal conductivities (e.g., average sedimentary pile conductivity > 2.75 $Wm^{-1}K^{-1}$) towards the Galilee Basin (Fig. 7).

5. Discussion

Several key points should be addressed when interpreting the data and their implications as well as model limitations. First, the validity of the model assumptions is examined. Subsequently, top down and bottom up effects, which may cause high heat flow, are discussed, followed by the spatial heat flow distribution and trends.

5.1. Validity of modelling assumption: Convection, Advection or Transient Heat Transfer

Poor agreement between observed temperature profiles and those predicted from 1D conductive heat flow models may indicate non-conductive heat transfer (e.g., Reid et al., 2012), such as convection, and/or advection, or transient heat transfer, or geometrical effects due to, for example, significant lateral gradients of topography, formation thickness, and material properties. Our results indicate that the mean temperature error is generally low (≤ 10°C, and in > 50% of the map, it is < 5°C, Figs.8a and 8b). In other words, the model error is on the order of the uncertainty imposed by poorly constrained material properties and that of the actual down-hole temperature measurements. Mean errors between 10 and 23°C occur only locally and may indicate areas that should be reassessed for their thermal transport processes. However, we conclude that 1D steady state conduction generally predicts the temperature data well at the regional scale (Figs.8a and 8b).

5.2. Top down effects: Sedimentary blanketing

Poorly conducting formations may trap heat by thermal refraction (e.g., Mildren and Sandiford, 1995). Fourier's law of heat conduction (1822) indicates a linear correlation between the geothermal gradient and the inverse of thermal conductivity:

$\frac{dT}{dz} = \frac{Q}{K}$ Eq. (4).

Therefore, one may expect to observe a positive correlation between the inverse of the mean thermal conductivity of the sedimentary cover and the predicted geothermal gradient. In our data, the coefficient of correlation is low (0.36) assuming a linear correlation. Similarly, no correlation between high temperature areas and total thickness of sediments is identified (correlation coefficient is 0.17). Our results suggest that high temperature areas are not associated with areas of low conductivity (Fig. 9) and thus sedimentary blanketing is not the cause of the elevated temperatures, at least not at the regional scale. This finding concurs with the study of Meixner et al. (2012) in the Cooper Basin, where elevated crustal or mantle inputs are required to explain observed temperatures.

5.3. Bottom up effects: Mantle versus Crustal Inputs

In the previous sections, convective, advective or transient heat transfer, and sedimentary blanketing have been ruled out as major contributors to elevated temperatures in SW Queensland. Consequently, a higher thermal input from depth is required, as suggested by Meixner et al. (2012). Mantle heat flow and radiogenic heat production of rocks below 5 km contribute to heat flow at 5 km depth. It is difficult to distinguish between mantle and crustal input if no independent constraints on either quantity are available. Mantle heat flow can be estimated through pressure-temperature estimates from xenoliths, which provide the geothermal gradient, and assuming a thermal conductivity for the mantle (e.g., peridotite). Alternatively, if the crustal structure and heat production of constituent rocks are known, the crustal contribution to heat flow at 5 km depth can be calculated (Perry et al., 2006). Since the estimated heat flow at 5 km depth is the sum of mantle and crustal contribution, one can be computed, if the other is known:

$Q_{5km} = Q_M + A_{ave}\,(z_M - z_{5km})$ Eq. (5),

where Q_{5km} is the heat flow at 5 km depth, Q_M is the mantle heat flow, z_{5km} is 5 km depth, z_M is the depth of the Moho and A_{ave} is the average radiogenic heat production between the Moho and z_{5km}.

Appendix A – Theoretical Approach

Our approach follows a modified version of Chapman (1986), with a different choice of boundary conditions. Like Chapman (1986), we assume a thermal steady state and treat each well as a 1D multi-layer diffusion problem. In the study area, most temperature data are located at a depth > 1 km, with very few data towards the surface of the Earth. We judge that the deeper temperature data are more reliable than the estimated surface temperature. Therefore, we calculate the temperature profiles stepwise from bottom to top rather than top to bottom as in Chapman (1986). Constant material properties are assumed in each layer. The only source term is radiogenic heat production. Conductive heat transfer through a single layer with a constant source term is described by the following ordinary differential equation (Chapman, 1986), also called Poisson's equation:

$$K \frac{d^2T}{dz^2} = -A \quad [A.1],$$

where K is the thermal conductivity [$Wm^{-1}K^{-1}$], T is the temperature [°C], z denotes depth [m], and A is the volumetric heat production (μWm^{-3}). Integrating Eq. (A.1) twice yields the temperature profile, a quadratic function:

$$K\,T(z) = -\frac{1}{2}Az^2 + zC_1 + C_2 \quad [A.2],$$

where C_1 and C_2 denote the integration constants. Because heat production is constant in the layer under consideration, the constants of this 1D equation can be solved for with the following boundary conditions:

$Q(z=z_B) = Q_B$

$T(z=z_B) = T_B$ [A.3],

where z_B denotes the vertical position of the layer bottom, Q_B is heat flow at the layer bottom, and T_B is temperature at the bottom. Thus, the temperature profile in the layer is:

$$T(z) = -\frac{A}{2K}\left(z^2 + z_B^2\right) + z\frac{Q_B + Az_B}{K} + T_B - \frac{z_B Q_B}{K} \quad [A.4].$$

The temperature profile through a multi-layer stack can now be computed easily by a piecewise (i.e., layer by layer) upward propagation of Eq. (A.4) with updated material properties and bottom temperature as well as heat flow. In other words, the temperature and heat flow at a layer interface are calculated for the lower layer with Eq. (A.4.) They serve as starting parameters for the temperature profile in the overlying layer, which is also calculated with Eq. (A.4) using updated material properties. This procedure requires that the temperature and heat flow at the bottom (or top) of the stack are known.

Constraints on the crustal structure in the study area are limited to deep crustal seismic transects including the Brisbane-Eromanga transect (Fig. 2) and for depths less than ca. 3 to 4 km by drill holes interception that penetrate the basement. The distribution of U, Th and K within the crust of the study area is largely unknown. Pressure and temperature information from young xenoliths are only available along the Eastern seaboard (O'Reilly and Griffin, 1990). Thus, available information to constrain the mantle heat flow across the temperature anomaly is very limited. The only estimated values for the mantle heat flow are located in South Australia and range from 25 to 29.5 mWm^{-2} (Neumann et al., 2000; McLaren et al., 2003; Meixner et al., 2012). Nevertheless, one can narrow down the possible range of mantle and crustal contributions to heat flow at 5 km depth by comparing Q_{5km} predicted by our stochastic approach to standard crustal and mantle heat flow values.

The depth of the Moho is well-established from the Brisbane-Eromanga seismic transect at ca. 40 km (Finlayson et al., 1990). Using eq. (4), we can determine the average crustal heat production required to match the interpreted heat flow at 5 km depth (Q_{5km}) given a particular mantle heat flow (Fig. 10).

The SW corner of Queensland is characterised by heat flow generally greater than 100 mWm^{-2} (Fig. 6b). Using Figure 10 and considering a mantle heat flow of 27 mWm^{-2} (Neumann et al., 2000; McLaren et al., 2003; Meixner et al., 2012), the average heat production between 5 and 40 km is much higher than crustal standards (e.g., ca. 2.1 to 3.3 μWm^{-3} compared to 0.87 and 1.65 μWm^{-3} for the average and upper continental crust, respectively; Fig. 10) suggesting that higher radiogenic crustal input is required.

It has recently been suggested that this region is characterised by a higher mantle heat flow, based on He isotope analyses of artesian water (Uysal et al., 2012). We can evaluate the mantle heat contribution by considering an extreme situation or environment such as a hot spot where mantle heat flow is expected to be the main contributor to the measured surface heat flow. Across the Hawaiian, hot spot for example, surface heat flow does not exceed 65 mWm^{-2} (Stein and Stein, 1993). Using this value as the mantle heat flow still requires higher than average crustal heat production values in the 5 to 40 km interval (e.g., ca. 1 to 2.2 μWm^{-3} versus 0.87 μWm^{-3} for the average continental crust) (Fig. 10). In addition, such high mantle heat flow would result in Moho temperatures in excess of 1000°C, which would lead to substantial melting of the lower crust (e.g., Thompson and Connolly, 1995) and drastic mechanical consequences. It is also inconsistent with Mareschal and Jaupart’s (2012) recent global analysis of the thermal regime of the continents, which predicts maximum Moho temperatures on the order of 800°C for crust of 40 km thickness.

The lower crust in the western part of the Eromanga transect is interpreted to be silicic (O'Reilly and Griffin, 1990). It is well recognised that silicic rocks have higher heat producing capacity than mafic rocks (Turcotte and Schubert, 2002). Consequently, our finding contradicts models that propose SW Queensland and the Thomson Orogen are underlain by oceanic crust (Harrington, 1974; Glen et al., 2013). We alternatively conclude that areas of high crustal temperature in SW Queensland require a silicic lower to middle crust located between 5 and 40 km depth and relatively enriched in heat producing elements.

It is well accepted that heat production becomes more depleted in the lower crust as a result of chemical differentiation of the continental crust through granitic magmatism (e.g., Taylor and McLennan, 1995; Rudnick and Gao, 2003; Hawkesworth and Kemp, 2006). Accordingly, models proposing an exponential decrease of heat production with depth (Lachenbruch, 1968) are sometimes invoked. These simple models are, however, in contradiction with heat production studies of drilled or exposed crustal profiles. Geochemical and geobarometric data indicate an exponential decrease of heat production with depth is rarely, if ever, valid, with high heat producing material often occurring at greater depth (Ashwal et al., 1987; Hart et al., 1990; Clauser et al., 1997; Brady et al., 2006; He et al., 2008). Such a crustal profile is exposed in the Arunta and Musgrave Inliers of central Australia where high heat producing material, characterized by the Mesoproterozoic Teapot Granite Complex (5.9 +/-1.7 μWm^{-3}), is abundant between pre-exhumation depths of 6 to 10 km (Sandiford et al., 2001). The deformation of Proterozoic crust during the Petermann and the Alice Springs orogenies (Sandiford et al., 2001) have led to exhumed blocks in the Musgrave and Arunta Inlier, and to buried and thrust downwards crustal material. Such high heat producing crustal material may therefore extend in the subsurface beneath the Thomson orogen at depth >5 km and is thus a likely candidate to explain the silicic and heat producing crust the model indicates.

5.4. SW-NE trend

The predicted heat flow map at 5 km depth (Figs. 6b and 11a) indicates a narrow SW-NE trending zone of lower heat flow with values ranging from 80 to 100 mWm^{-2}. In response to the linear relationship between the average heat production at 5 to 40 km and heat flow (Eq. (5)), this trend also corresponds to heat production at 5 to 40 km that are lower than average.

This zone of lower heat flow seems to coincide remarkably well with structural trends observed in seismic horizons (Fig. 11b) related to the top of the Cadna-Owie formation (Radke, 2009) and to thick sedimentary cover (Fig. 3). Specifically, the low heat flow trend corresponds to the Arraburry and Windorah troughs and the Ullenbury and Thomson depressions (Fig. 2). A lower heat flow value in this area could result from localised lower mantle heat flow or a local decrease in radiogenic heat production. The latter case would occur if the depressions were related to a more mafic crust or to thinned continental crust. The latter is consistent with the observed increase in sedimentary infill in the troughs. Tectonic extension will reduce the vertical extent of crystalline basement, which is potentially enriched in high heat producing elements, and thus the local crustal contribution to heat flow.

6. Conclusions

This study has re-evaluated the geothermal potential in SW Queensland and has confirmed the generally high subsurface temperatures observed in Oztemp. A new temperature map at 5 km depth reveals a strong SW-NE trend of elevated (200-250°C) temperatures. This study has also investigated the geological controls on the elevated geothermal gradients using a stochastic approach. Estimated temperature and heat flow at 5 km depth are most sensitive to the thermal conductivity of the strata. A poor correlation between thickness and average thermal conductivity of the sedimentary pile and estimated temperature at 5 km depth suggests that thermal blanketing is not the sole cause of high geothermal gradients. In addition, the small mean temperature errors between modelled and observed temperature profiles indicate that the assumption of steady state, purely conductive heat transfer may be valid and that effects of advective, convective or transient heat transfer are likely to be minor at the regional scale of this study.

Consequently, elevated subsurface temperatures must result from bottom up contributions. Estimations of the relative contributions of mantle versus crustal heat input from below 5 km depth suggest that the observed high geothermal gradients are unlikely to be generated by elevated mantle heat flow alone. Consequently, we conclude that the crust between 5 and 40 km depth is relatively high heat producing in the region of anomalously high crustal temperatures. Our study supports the existence of silicic continental lower to middle crust enriched in heat producing elements beneath the region of elevated temperature and for much of the Thomson orogen. A SW-NE trend of lower heat flow and inferred average heat production through the study area correlates with structural trends and may relate to zones of thinned continental crust and therefore lower total crustal heat production.

Acknowledgements

C. Siégel is supported by the QUT Postgraduate Research Award. C. Siégel acknowledges support from QGECE and IFE for funding analytical experiments. We thank A. Antriasian and S. Egan for thermal conductivity measurements, A. Greig for ICPMS analysis of U, Th and K and ALS for XRF analysis of K_2O. O. Gaede, T. Uysal, A. Kirkby and T. Meixner are thanked for discussions. Two anonymous reviewers and the editor J. Moore are thanked for providing comments that have significantly improved the manuscript.

In this study, we estimated the temperature T_T and heat flow Q_T at a depth of z_T = 5 km for each well. No well in the study area has penetrated the crust to this depth, and the maximum well depth is 3.9 km (PPC Lissoy 1). However, for each well, the number of intersected formations and their respective thicknesses, conductivities and heat production rates are known or can be estimated (see section 3.2 for discussion of material properties and their derivation) to a certain depth $z_C < z_T$. Well logs also provide often sparse temperature measurements, which provide an estimated true formation temperature when corrected (see section 3.2.3 for a discussion of temperature methods and corrections). Assuming that the material between the deepest observation in the well and z_T remains identical, T_T and Q_T can be inverted by minimising the mean squared temperature error of the calculated temperature profile (Fig. 2):

$$\Delta\varepsilon = \sum_{i=1}^{N} \frac{(Ti-ti)^2}{N} \quad [A.5],$$

where N denotes the number of actual temperature observations in the well, *Ti* is the measured temperature at a given depth, and *ti* is the predicted temperature at that depth. For a given Q_T, it is straightforward to calculate the best-fit T_T.

Eq. (A.4) indicates that the choice of the initial T_B controls the position of the temperature profile (it is a simple summand) and thermal conductivity controls the shape of the temperature profile (it affects the slope of the linear part of Eq. (A.4)). A change of T_T would therefore simply shift the temperature profile by its magnitude along the temperature axis (Fig. A.1). Thus, T_T can be computed by minimising the mean squared temperature error (Fig. A.1):

$$\Delta\varepsilon = \sum_{i=1}^{N} \frac{(Ti-(ti+X))^2}{N} \quad [A.6],$$

and with $\Delta Ti = (Ti - ti)$:

$$\Delta\varepsilon = X^2 - \frac{2}{N} X \sum_{i=1}^{N} \Delta Ti + \frac{1}{N} \sum_{i=1}^{N} \Delta Ti^2 \quad [A.7].$$

Eq. (A.7) has the minimum:

$$\Delta\varepsilon' = 2X - \frac{2}{N} \sum_{i=1}^{N} \Delta Ti = 0 \quad [A.8].$$

Therefore, the following solution for T_T is obtained:

$$X = \sum_{i=1}^{N} \frac{\Delta Ti}{N} \quad [A.9].$$

The minimised square temperature error can hence be expressed using Eq.(A.7) and (A.9):

$$\Delta\varepsilon = \sum_{i=1}^{N} \frac{(Ti-(ti+\sum_{i=1}^{N}\frac{\Delta Ti}{N}))^2}{N} \text{ [A.10].}$$

This procedure requires that Q_T is known, which is not the case. Eq. (A.10) shows that $\Delta\varepsilon$ is a quadratic function of Q_T:

$$f(Q_T) = \Delta\varepsilon = aQ_T^2 + bQ_T + c \text{ [A.11].}$$

Given three points, $P_j(Q_{Tj}/\ \Delta\varepsilon_j)$, the coefficients a, b and c of this quadratic function can be calculated empirically and the best fit Q_T determined by minimisation. Thus, both the best-fit temperature profile and the respective temperature and heat flow at 5 km depth are determined in a three step process for any given well: first, three arbitrary Q_T are assumed (0, 50, and 100 µWm^{-3}). For each one, the corresponding best-fit T_T and its mean squared temperature error are calculated analytically with Eqs. (A.9) and (A.10). This yields the desired three pairs of Q_T and $\Delta\varepsilon$ data needed to calculate the coefficients of Eq. 11. The best-fit Q_T is simply the minimum of Eq. (A.11): -b(2a)$^{-1}$. In the third step, the corresponding T_T is computed for the best-fit Q_T with Eq. (A.9).

References

Ashwal, L. D., P. Morgan, S. A. Kelley and J. A. Percival (1987). "Heat production in an Archean crustal profile and implications for heat flow and mobilization of heat-producing elements." Earth and Planetary Science Letters **85**(4): 439-450.

Bahadori, A., S. Zendehboudi and G. Zahedi (2013). "A review of geothermal energy resources in Australia: Current status and prospects." Renewable and Sustainable Energy Reviews **21**(0): 29-34.

Bauer, M. S. and D. S. Chapman (1986). "Thermal regime at the Upper Stillwater dam site, Uinta mountains, Utah: Implications for terrain, microclimate and structural corrections in heat flow studies." Tectonophysics **128**(1–2): 1-20.

Beardsmore, G. (2004). "The influence of basement on surface heat flow in the Cooper Basin." Exploration Geophysics (Melbourne) **35**(4): 223-235.

Beardsmore, G. R. and J. P. Cull (2001). Crustal heat flow: a guide to measurement and modelling, Cambridge University Press.

Birch, F. and H. Clark (1940). "The thermal conductivity of rocks and its dependence upon temperature and composition; Part II." American Journal of Science **238**(9): 613-635.

Brady, R. J., M. N. Ducea, S. B. Kidder and J. B. Saleeby (2006). "The distribution of radiogenic heat production as a function of depth in the Sierra Nevada Batholith, California." Lithos **86**(3–4): 229-244.

Brown, D. D., P. A. Carr and D. J. Purdy (2012). Database of basement drill holes in the Thomson Orogen and Roma Shelf regions, Queensland. Brisbane, Geological Survey of Queensland. **GSQ record 2012/06**.

Budd, A., F. Holgate, E. Gerner and B. Ayling (2006). In search of the next hotspot. AusGeo.

Champion, D. C., A. Budd and L. Wyborn (2007). OZCHEM National Whole-Rock Geochemistry Database., Geoscience Australia, http://www.ga.gov.au/meta/ANZCW0703011055.html.

Chapman, D. S. (1986). "Thermal gradients in the continental crust." Geological Society Special Publications **24**: 63-70.

Chapman, D. S., T. Keho, M. S. Bauer and M. D. Picard (1984). "Heat flow in the Uinta Basin determined from bottom hole temperature (BHT) data." Geophysics **49**(4): 453-466.

Chopra, P. and F. Holgate (2005). "A GIS Analysis of Temperature in the Australian Crust." Proceedings World Geothermal Congress Antalya, Turkey, 24-29 April 2005.

Clauser, C., P. Giese, E. Huenges, T. Kohl, H. Lehmann, L. Rybach, J. Šafanda, H. Wilhelm, K. Windloff and G. Zoth (1997). "The thermal regime of the crystalline continental crust: implications from the KTB." Journal of Geophysical Research: Solid Earth (1978–2012) **102**(B8): 18417-18441.

Clauser, C. and E. Huenges (1995). "Thermal conductivity of rocks and minerals." AGU Reference Shelf **3**: 105-126.

Cook, A. G., S. E. Bryan and J. J. Draper (2013). Post-orogenic Mesozoic basins and magmatism. Geology of Queensland. P. Jell. Brisbane, QLD, Geological Survey of Queensland.

Dowd, A.-M., N. Boughen, P. Ashworth and S. Carr-Cornish (2011). "Geothermal technology in Australia: Investigating social acceptance." Energy Policy **39**(10): 6301-6307.

Draper, J. J. (2006). "The Thomson Fold Belt in Queensland revisited." ASEG Extended Abstracts.

Draper, J. J. and R. D'Arcy (2006). "Geothermal potential in Queensland." Queensland Government Mining Journal: 80-83.

Fergusson, C. L. and R. A. Henderson (2013). Thomson Orogen. Geology of Queensland. P. Jell. Brisbane, QLD, Geological Survey of Queensland.

Ferrero, C. and K. Gallagher (2002). "Stochastic thermal history modelling. 1. Constraining heat flow histories and their uncertainty." Marine and Petroleum Geology **19**(6): 633-648.

Finlayson, D. (1990). Basin and crustal evolution along the Eromanga-Brisbane Geoscience Transect: precis and analogues. The Eromanga–Brisbane Geoscience Transect: a guide to basin development across Phanerozoic Australia in southern Queensland. D. Finlayson, Bureau of Mineral Resources Bulletin. **232:** 253-261.

Finlayson, D., J. Leven, K. Wake-Dyster and D. Johnstone (1990). A crustal image under the basins of southern Queensland along the Eromanga–Brisbane Geoscience Transect. The Eromanga–Brisbane Geoscience Transect: a guide to basin development across Phanerozoic Australia in southern Queensland. D. M. Finlayson, Bureau of Mineral Resources Bulletin. **232:** 153-175.

Förster, A., D. F. Merriam and J. C. Davis (1997). "Spatial analysis of temperature (BHT/DST) data and consequences for heat-flow determination in sedimentary basins." Geologische Rundschau **86**(2): 252-261.

Fourier, J. B. J. (1822). Théorie analytique de la chaleur. Paris, F. Didot.

Gallagher, K. (1987). "Thermal conductivity and heat flow in the Southern Cooper Basin." Exploration Geophysics **18**(2): 62-65.

Gatehouse, C. G., C. M. Fanning and R. B. Flint (1995). "Geochronology of the Big Lake Suite, Warburton Basin, northeastern South Australia." Quarterly Geological Notes - Geological Survey of South Australia **128**: 8-16.

Gerner, E. J. and F. L. Holgate (2010). OzTemp - interpreted temperature at 5km depth image. Canberra, Geoscience Australia, http://www.ga.gov.au/meta/ANZCW0703014335.html.

Glen, R., R. Korsch, R. Hegarty, A. Saeed, Y. P. Djomani, R. Costelloe and E. Belousova (2013). "Geodynamic significance of the boundary between the Thomson Orogen and the Lachlan Orogen, northwestern New South Wales and implications for Tasmanide tectonics." Australian Journal of Earth Sciences **60**(3): 371-412.

Goutorbe, B., F. Lucazeau and A. Bonneville (2006). "Using neural networks to predict thermal conductivity from geophysical well logs." Geophysical Journal International **166**(1): 115-125.

Goutorbe, B., F. Lucazeau and A. Bonneville (2007). "Comparison of several BHT correction methods: A case study on an Australian data set." Geophysical Journal International **170**(2): 913-922.

Goutorbe, B., F. Lucazeau and A. Bonneville (2008). "Surface heat flow and the mantle contribution on the margins of Australia." Geochemistry, Geophysics, Geosystems **9**(5).

Harrington, H. J. (1974). The Tasman Geosyncline in Australia. The Tasman geosyncline—a symposium in honour of Professor Dorothy Hill, Geological Society of Australia, Queensland Division.

Hart, R. J., M. A. G. Andreoli, M. Tredoux and M. J. De Wit (1990). "Geochemistry across an exposed section of Archaean crust at Vredefort, South Africa: with implications for mid-crustal discontinuities." Chemical Geology **82**(0): 21-50.

Hawkesworth, C. J. and A. I. S. Kemp (2006). "Evolution of the continental crust." Nature **443**(7113): 811-817.

He, L., S. Hu, S. Huang, W. Yang, J. Wang, Y. Yuan and S. Yang (2008). "Heat flow study at the Chinese Continental Scientific Drilling site: Borehole temperature, thermal conductivity, and radiogenic heat production." Journal of Geophysical Research: Solid Earth (1978–2012) **113**(B2).

Henderson, R. (1980). "Structural outline and summary geological history for northeastern Australia." The geology and geophysics of northeastern Australia: 1–26.

Holgate, F. L. and E. J. Gerner (2011). OZTemp Well Temperature Data Geoscience Australia, http://www.ga.gov.au/meta/ANZCW0703013802.html.

Kamber, B. S., A. Greig and K. D. Collerson (2005). "A new estimate for the composition of weathered young upper continental crust from alluvial sediments, Queensland, Australia." Geochimica Et Cosmochimica Acta **69**(4): 1041-1058.

Kirkby, A. L. and E. J. Gerner (2010). Heat flow interpretations for the Australian continent: Release 1, Geoscience Australia. **Record 2010/41:** 28p.

Korsch, R. J., H. I. M. Struckmeyer, A. Kirkby, L. J. Hutton, L. K. Carr, K. L. Hoffmann, R. Chopping, I. G. Roy, M. Fitzell, J. M. Totterdell, M. G. Nicoll and B. Talebi (2011). "Energy potential of the Millungera Basin; a newly discovered basin in north Queensland." APPEA Journal **51**: 295-332.

Kutasov, I. and L. Eppelbaum (2009). "Estimation of geothermal gradients from single temperature log-field cases." Journal of Geophysics and Engineering **6**(2): 131.

Lachenbruch, A. H. (1968). "Preliminary geothermal model of the Sierra Nevada." Journal of Geophysical Research **73**(22): 6977-6989.

Lund, J. W. and T. Boyd (1999). "Small geothermal power project examples." Geo-Heat Center Quarterly Bulletin **20**(2): 9-26.

Mareschal, J.-C. and C. Jaupart (2012). "Radiogenic Heat Production, Thermal Regime and Evolution of Continental Crust." Tectonophysics.

Marshall, V. J. (2013). Petrological, geochemical and geochronological characterisation of heat-producing granites. Brisbane, The University of Queensland. **M.Sc.**

Matthews, C. (2009). "Geothermal energy prospectivity of the Torrens Hinge Zone: evidence from new heat flow data." Exploration Geophysics **40**(3): 288-300.

Maze, G. and U. Wagner (2009). "A Note on the Weighted Harmonic-Geometric-Arithmetic Means Inequalities." arXiv preprint arXiv:0910.0948.

McLaren, S., M. A. Sandiford, M. P. Hand, N. L. Neumann, L. Wyborn and I. Bastrakova (2003). The hot southern continent: heat flow and heat production in Australian Proterozoic terranes. Evolution and Dynamics of the Australian Plate. R. R. Hillis and D. Muller, Special Publications Geological Society of Australia. **Chapter 12:** 151-161.

Meixner, A. J., A. L. Kirkby, D. T. Lescinsky and N. Horspool (2012). The Cooper Basin 3D map version 2; thermal modelling and temperature uncertainty, Geoscience Australia, Canberra, A.C.T., Australia.
Middleton, M. F. (1979). "Heat flow in the Moomba, Big lake and Toolachee gas fields of the Cooper Basin and implications for hydrocarbon maturation." Exploration Geophysics **10**: 149-155.
Mildren, S. D. and M. Sandiford (1995). "Heat refraction and low-pressure metamorphism in the northern Flinders Ranges, South Australia." Australian Journal of Earth Sciences **42**(3): 241-247.
Murray, C. (1994). "Descriptions of basement cores from selected petroleum exploration wells and stratigraphic bores in Queensland." Queensland Geological Record **10**.
Murray, C. G. (1994). Basement cores from the Tasman Fold Belt System beneath the Great Arterian Basin in Queensland. Q. Government, Geological Survey of Queensland. **Record 1994/10**.
Neumann, N., M. Sandiford and J. Foden (2000). "Regional geochemistry and continental heat flow: implications for the origin of the South Australian heat flow anomaly." Earth and Planetary Science Letters **183**(1-2): 107-120.
O'Reilly, S. Y. and W. L. Griffin (1990). Geophysical and petrologic properties of the crust/mantle boundary region, eastern Australia; relevance to the Eromanga-Brisbane Transect. The Eromanga–Brisbane Geoscience Transect: a guide to basin development across Phanerozoic Australia in southern Queensland. D. M. Finlayson, Bureau of Mineral Resources Bulletin. **232:** 203-212.
Perry, H. K. C., C. Jaupart, J. C. Mareschal and G. Bienfait (2006). "Crustal heat production in the Superior Province, Canadian Shield, and in North America inferred from heat flow data." Journal of Geophysical Research: Solid Earth **111**(B4): B04401.
Pirlo, M. C. (2002). "The silica heat flow interpretation technique: application to continental Australia." Journal of Volcanology and Geothermal Research **115**(1–2): 19-31.
Polak, E. J. and C. J. Horsfall (1979). "Geothermal gradients in the Great Artesian Basin, Australia." Bulletin - Australian Society of Exploration Geophysicists **9**(4): 184.
Purdy, D. J., P. A. Carr and D. D. Brown (2013). Review of the geology, mineralisation and geothermal potential of the Thomson Orogen. Brisbane, Geological Survey of Queensland. **GSQ record 2013/01**.
Radke, B. (2009). Hydrocarbon and geothermal prospectivity of sedimentary basins in central Australia; Warburton, Cooper, Pedirka, Galilee, Simpson and Eromanga Basins, Geoscience Australia, Canberra, A.C.T., Australia.
Reid, L. B., G. Bloomfield, L. P. Ricard, C. Botman and P. Wilkes (2012). "Shallow geothermal regime in the Perth Metropolitan Area." Australian Journal of Earth Sciences **59**(7): 1033-1048.
Ricard, L. P. and J. B. Chanu (2013). "GeoTemp™ 1.0: A MATLAB-based program for the processing, interpretation and modelling of geological formation temperature measurements." Computers and Geosciences.
Rudnick, R. L. and S. Gao (2003). Composition of the Continental Crust. Treatise on Geochemistry. D. H. Heinrich and K. T. Karl. Oxford, Pergamon**:** 1-64.
Rybach, L. and G. Buntebarth (1981). "Heat-generating radioelements in granitic magmas." Journal of Volcanology and Geothermal Research **10**(4): 395-404.
Sandiford, M., M. Hand and S. McLaren (2001). "Tectonic feedback, intraplate orogeny and the geochemical structure of the crust: a central Australian perspective." Special Publication - Geological Society of London **184**: 195-218.
Sass, J. H., A. H. Lachenbruch, T. H. Moses, Jr. and P. Morgan (1992). "Heat flow from a scientific research well at Cajon Pass, California." Journal of Geophysical Research **97**(B4): 5017-5030.
Schilling, O., H. A. Sheldon, L. B. Reid and S. Corbel (2013). "Hydrothermal models of the Perth metropolitan area, Western Australia: Implications for geothermal energy." Hydrogeology Journal **21**(3): 605-621.
Seipold, U. (1998). "Temperature dependence of thermal transport properties of crystalline rocks—a general law." Tectonophysics **291**(1): 161-171.
Sheldon, H. A., B. Florio, M. G. Trefry, L. B. Reid, L. P. Ricard and K. A. R. Ghori (2012). "The potential for convection and implications for geothermal energy in the Perth Basin, Western Australia." Hydrogeology Journal **20**(7): 1251-1268.
Somerville, M., D. Wyborn, P. Chopra, S. Rahman, D. Estrella and T. Van der Meulen (1994). Hot dry rocks feasibility study, Energy Research and Development Corporation.
Srivastava, K. (2005). "Modelling the variability of heat flow due to the random thermal conductivity of the crust." Geophysical Journal International **160**(2): 776-782.
Srivastava, K. and R. N. Singh (1999). "A stochastic model to quantify the steady-state crustal geotherms subject to uncertainties in thermal conductivity." Geophysical Journal International **138**(3): 895-899.
Stein, C. A. and S. Stein (1993). "Constraints on Pacific midplate swells from global depth-age and heat flow-age models." The Mesozoic Pacific: geology, tectonics, and volcanism: 53-76.
Taylor, S. R. and S. M. McLennan (1995). "The geochemical evolution of the continental-crust." Reviews of Geophysics **33**(2): 241-265.

Thompson, A. B. and J. A. Connolly (1995). "Melting of the continental crust: some thermal and petrological constraints on anatexis in continental collision zones and other tectonic settings." Journal of Geophysical Research **100**(B8): 15565-15515,15579.

Turcotte, D. L. and G. Schubert (2002). Geodynamics. Cambridge, Cambridge University Press.

Uysal, T. I., C. Siégel, G. Yuce and F. Italiano (2012). Great Artesian Basin Heat Source Characterisation in the light of recent isotope studies. Proceedings of the 2012 Australian Geothermal Energy Conference. C. Huddlestone-Holmes and E. Gerner. Canberra, Geoscience Australia. **Record 2012/73:** 207-209.

Withnall, I. W. and L. J. Hutton (2013). North Australian Craton. Geology of Queensland. P. Jell. Brisbane, QLD, Geological Survey of Queensland.

Yorath, C. J. and R. D. Hyndman (1983). "Subsidence and thermal history of Queen Charlotte Basin." Canadian Journal of Earth Sciences **20**(1): 135-159.

Zoth, G. and R. Haenel (1988). Appendix. Handbook of Terrestrial Heat-Flow Density Determination. Dordrecht, Kluwer Academic Publishers**:** 449-466.

Table 1

Symbol	Parameter
K	Thermal Conductivity [$Wm^{-1}K^{-1}$]
A	Heat Production [μWm^{-3}]
T	Temperature [°C]
T_B	Temperature at 5 km depth [°C]
z	Depth [m]
z_B	Depth of the bottom of the layer [m]
z_T	Depth equivalent to 5 km [m]
C_1 and C_2	Constants derived from integration
Q	Heat Flow [mWm^{-2}]
Q_B	Heat flow at the bottom of the layer [mWm^{-2}]
Q_T	Heat flow at 5 km depth [mWm^{-2}]
$\Delta\varepsilon$	Mean squared temperature error
$\Delta\varepsilon$'	Derivative of the mean squared temperature error
$P_j(Q_{Tj}/ \Delta\varepsilon_j)$	Point P_j with attribute Q_{Tj} and $\Delta\varepsilon_j$ used to determine coefficients of the quadratic function
N	Number of observed temperatures
T_i	Measured temperature at a given depth [°C]
t_i	Predicted temperature at a given depth [°C]
T_T	Estimated temperature at 5 km depth [°C]
ΔTi	Difference between measured and predicted temperature at a given depth [°C]
Kb	Bulk thermal conductivity [$Wm^{-1}K^{-1}$]
Km	Matrix conductivity [$Wm^{-1}K^{-1}$]
ϕ	Porosity [Vol. %]
K(25)	Thermal conductivity at 25°C [$Wm^{-1}K^{-1}$]
$T_{B\infty}$	True formation temperature [°C]
$T_B(t)$	temperature at the bottom of the hole at a particular time [°C]
t_c	circulation time [s]
t_e	time elapsed since the fluids circulated [s]
C	slope determined by the BHT measurements
C_U	Bulk rock concentration of Uranium [ppm]
C_{Th}	Bulk rock concentration of Thorium [ppm]
C_{K2O}	Bulk rock concentration of Potassium oxide [wt%]
ρ	Density [kgm^{-3}]

Table 2

Formation Name	Formation Age	Thickness range (m)		Estimated thermal conductivity ($Wm^{-1}K^{-1}$)	n*	Measured thermal conductivity ($Wm^{-1}K^{-1}$) (RSD****)	n*	Thermal conductivity References
		All wells	*This study (n*=163)*					
Surface Deposits	Quaternary	-	2-247	2.30±2.00**	-	-	-	-
Tertiary Volcanics	Tertiary	-	10-44	1.73±0.21***	-	-	-	-
Eromanga Basin								
Winton Formation	Late Cretaceous	16-1030	34-1166	2.78±0.22	3	1.48±0.06 (04)	2	b
Mackunda Formation	Early Cretaceous	31-1030	34-257	2.90±0.14	3	1.35±0.25 (19)	1	b
Allaru Mudstone	Early Cretaceous	2-453	31-360	2.52±0.51	3	1.39±0.32 (23)	10	a; b; d; f
Toolebuc Formation	Early Cretaceous	1-23	1-173	2.48±0.51	3	1.06±0.29 (27)	4	e; f
Walumbilla Formation	Early Cretaceous	0.1-1552	23-499	2.51±0.46	7	1.43±0.42 (29)	22	a; d; e; f
Cadna-Owie Formation	Early Cretaceous	3-1090	26-267	3.03±0.33	4	1.86±0.23 (12)	6	a; b; c
Hooray Sandstone	Late Jurassic-Early Cretaceous	13-462	38-211	3.10±0.42	4	2.59±0.74 (29)	2	e; d
Westbourne Formation	Late Jurassic	4-3273	3-382	3.31±0.66	7	2.92±0.91 (31)	10	b; c; e; d
Adori Sandstone	Late Jurassic	2-126	5-119	3.48±0.91	4	4.63±0.35 (8)	2	b
Birkhead Formation	Middle Jurassic	3-451	10-148	2.28±0.68	4	3.90±1.28 (33)	9	a; b
Hutton Sandstone	Middle Jurassic	1-680	11-294	3.27±0.46	7	4.67±0.83 (18)	14	a; b; c
Poolowanna Formation	Early Jurassic	4-371	10-220	3.28±0.55	3	3.94±2.11 (54)	4	b
Precipice Sandstone	Early Jurassic	1-1447	4-122	3.94±1.38	3	-	-	-
Surat Basin								
Griman Creek Formation	Early Cretaceous	13-397	167-307	2.78±0.22	3	-	-	-
Surat Siltstone	Early Cretaceous	14-391	97-155	2.90±0.07	3	-	-	-
Walumbilla Formation	Early Cretaceous	0.1-1552	23-499	2.51±0.46	7	-	-	-
Bungil Formation	Early Cretaceous	1-702	35-287	3.25±0.29	3	-	-	-
Mooga Sandstone	Late Jurassic – Early Cretaceous	5-902	33-310	3.33±0.29	3	-	-	-
Orallo Formation	Late Jurassic	4-385	101-266	3.40±0.18	3	1.99±0.16 (08)	7	e
Gubberamunda Sandstone	Late Jurassic	7-488	35-259	3.65±0.06	3	2.58±0.17 (07)	1	e
Westbourne Formation	Late Jurassic	4-3273	3-382	3.05±0.24	7	-	-	-
Springbok Sandstone	Middle Jurassic	2-338	25-112	3.56±0.24	3	-	-	-
Walloon Coal Measures	Middle Jurassic	31-861	114-446	2.82±0.16	3	-	-	-
Eurombah Formation	Middle Jurassic	3-337	25-79	3.49±0.11	3	-	-	-
Hutton Sandstone	Middle Jurassic	1-680	11-294	3.30±0.21	7	4.67±0.83 (18)	14	a; b; c
Evergreen Formation – Upper unit	Early Jurassic	10-271	15-181	2.85±0.13	3	-	-	-
Boxvale Sandstone	Early Jurassic	1-129	1-81	3.26±0.68	3	-	-	-
Evergreen Formation – Lower unit	Early Jurassic	2-127	19-195	3.16±0.13	3	-	-	-
Precipice Sandstone	Late Triassic – Early Jurassic	1-1447	4-122	3.94±1.38	3	-	-	-
Cooper Basin								
Nappamerri Group	Late Permian – Middle Triassic	3-494	23-460	3.11±0.18	3	3.42±1.11 (32)	9	a; b; c
Gidgealpa Group: Toolachee Formation	Middle – Late Permian	3-367	8-145	2.70±0.74	3	2.93±1.32 (45)	11	a; b; c
Gidgealpa Group: Daralingie Formation	Early Permian	6-96	8-96	2.42±0.27	3	2.80±1.19 (43)	8	b; c
Gidgealpa Group: Roseneath Shale	Early – Middle Permian	2-183	3-98	2.45±0.46	3	1.90±0.40 (21)	4	a; b; c
Gidgealpa Group: Epsilon Formation	Early Permian	2-265	5-90	2.46±0.72	3	2.44±1.55 (64)	5	a; b; c

	Murteree Shale	Early Permian	3-521	4-59	2.63±1.00	3	2.59±0.85 (33)	4	a; b
	Patchawarra Formation	Early Permian	1-404	3-383	2.61±0.91	3	3.62±1.61 (44)	11	a; b; c
	Tirrawarra sandstone	Early Permian	31-88	33-40	5.14±0.80	3	3.95±1.07 (27)	6	b; c
	Merrimelia Formation	Early Permian	9-201	9-70	3.21±0.58	3	3.60±0.86 (24)	6	a; b; c
Galilee Basin									
Moolayember Formation		Late Triassic	2-1063	9-602	2.94±0.59	4	-	-	-
Warang Sandstone		Early – Middle Triassic	394	149	3.57±1.35	3	-	-	-
Betts Creek Beds		Late Permian	21-215	111-253	2.65±0.96	3	-	-	-
Clematis Sandstone		Early – Middle Triassic	4-581	1-190	3.45±0.32	4	-	-	-
Rewan Group		Late Permian – Early Triassic	2-1302	43-591	2.87±0.15	3	-	-	-
Bandanna Formation		Late Permian	1-1036	12-818	2.88±0.54	4	-	-	-
Back Creek Group	Black Alley Shale	Late Permian	5-373	11-191	3.43±1.00	3	1.73±0.23 (13)	2	g
Back Creek Group	Peawaddy Formation	Late Permian	5-349	21-188	3.03±0.25	3			
Back Creek Group	Catherine Sandstone	Middle Permian	2-178	27-131	3.88±0.90	3			
Back Creek Group	Ingelara Formation	Late Permian	10-309	32-173	2.96±0.25	3			
Back Creek Group	Freitag Formation	Late Permian	4-214	17-127	3.76±1.04	3			
Back Creek Group	Aldebaran Formation	Early – Middle Permian	11-908	183-1086	3.98±0.92	3			
Cattle Creek Formation		Early Permian	17-891	85-829	3.11±0.22	3	-	-	-
Reids Dome Beds		Early Permian	63-1263	26-667	2.80±0.49	3	-	-	-
Colinlea Sandstone		Late Permian	2-966	13-91	3.72±0.15	3	-	-	-
Aramac Coal Measures		Early Permian	18-333	18-232	3.29±0.44	3	-	-	-
Jochmus Formation – Upper unit		Late Carboniferous – Early Permian	287	17-319	3.71±1.04	4	-	-	-
Eddie Tuff Member		Early Permian	85-125	21-125	3.38±1.41	3	-	-	-
Jochmus Formation – Lower unit		Late Carboniferous – Early Permian	341-400	12-341	3.06±0.33	3	-	-	-
Jericho Formation – Upper unit		Late Carboniferous – Early Permian	200	63-400	2.98±0.57	3	-	-	-
Oakleigh Siltstone Member		Late Carboniferous – Early Permian	46-167	69-167	2.62±0.79	3	-	-	-
Jericho Formation – Lower unit		Late Carboniferous – Early Permian	-	126-386	3.03±0.48	3	-	-	-
Lake Galilee Sandstone		Late Carboniferous – Early Permian	287	85-287	4.21±0.53	3	-	-	-
Drummond Basin									
Ducabrook Formation		Early Carboniferous	12-43	1025	3.59	1	-	-	-
Natal Formation		Early Carboniferous	206-384	385	2.85	1	-	-	-
Bulliwallah Formation		Early Carboniferous	43-657	656	3.02	1	-	-	-
Star of Hope Formation		Early Carboniferous	377-890	890	3.24	1	-	-	-
Raymond Formation		Early Carboniferous	264-417	417	3.05	1	-	-	-
Scartwater Formation		Early Carboniferous	441	442	3.08	1	-	-	-
Saint Annes Formation		Late Devonian – Early Carboniferous	214	214	3.47	1	-	-	-
Ukalunka Beds		Early Devonian	-	395	3.04	1	-	-	-
Adavale Basin									
Buckabie Formation		Late Devonian – Early Carboniferous	37-1743	8-1251	3.21±0.17	3	-	-	-
Etonvale Formation		Middle Devonian	12-704	5-415	3.52±1.04	3	-	-	-
Cooladdi Formation		Middle Devonian	6-64	16	4.15±0.19	3	-	-	-
Lissoy Sandstone		Middle Devonian	31-53	44	3.90±0.86	3	-	-	-
Bury Limestone		Middle Devonian	217-328	253-301	3.01±0.63	3	-	-	-

Log Creek Formation	Middle Devonian	59-263	317-657	3.28±0.36	3	-	-	-
Georgina Basin								
Toko Group	Ordovician	-	220-1190	3.84±0.70	3	-	-	-
Cockroach Group	Late Cambrian – Early Ordovician	-	146-1135	4.03±0.46	3	-	-	-
Narpa Group	Early – Late Cambrian	-	209-1283	3.19±0.78	3	-	-	-
Shadow Group	Middle Cambrian – Proterozoic	-	7-513	3.57±0.57	3	-	-	-

* n is the number of samples
** Surface deposits are considered as typical sediments (from Beardsmore and Cull, 2001; refer to Electronic Appendix A)
*** Tertiary Volcanics are considered as basalt (from Beardsmore and Cull, 2001; refer to Electronic Appendix A)
**** RSD is Relative Standard Deviation
a Gallagher (1987)
b Hot Dry Rocks Pty Ltd, G. E. C. (2011)
c Weber and Kirkby (2011)
d Brown et al. (2012)
e Faulkner et al. (2012)
f Fitzell et al. (2012)
g Troup et al. (2012)

Table 3

Sample	Depth (m)	Description	Modal Mineralogy						Thermal conductivity
			Q	AF	Pl	Ms	Bt	Hb	(W/mK)
DIO Wolgolla 1	2040.4-2041.7	Altered, leucocratic, coarse-grained, porphyritic, muscovite-biotite S-type monzogranite	35	30	30	3	2		3.55+/-0.07
TEA Roseneath 1	2192-2196	Pale grey, medium-grained, leucocratic, biotite-muscovite S-type monzogranite; cut by black veins	35	28	30	5	2		3.70+/-0.06
AOD Budgerygar 1	1621.5-1622.4	Grey, medium-grained, equigranular, hornblende-biotite I-type monzogranite	30	25	25		10	10	3.30+/-0.09
LOL Stormhill 1	1552-1553	Pale grey, medium-grained, equigranular, biotite I-type monzogranite	30	40	25		5		3.40+/-0.04
AOP Balfour 1	1693-1695	Red, fine-grained, equigranular, I-type tonalite; Enclaves and calcite veins	30		40			30	2.90+/-0.16
TEP Jandowae West 1	467-468	Pale grey, medium-grained, equigranular, bornblende-biotite I-type quartz monzodiorite	10	10	45		15	20	2.51+/-0.24
Javel 2*	1146-1176	Pale grey to pink, coarse-grained, porphyritic, biotite-muscovite S-type monzogranite	30	40	20	2	8		3.68+/-0.19
PGA Bradley 1	890.6-894.4	Red, medium-grained, porphyritic, biotite I-type monzogranite	30	30	35		5		3.55+/-0.05

* Upper granite

Q is Quartz, AF is Alkali Feldspar, Pl is plagioclase, Ms is Muscovite, Bt is Biotite and Hb is Hornblende

Table 4

Lithology	SiO_2 (wt%)	U (ppm)	Th (ppm)	K_2O (wt%)	Heat production ($\mu W/m^3$)*	Data sources
Sediments	65.9	3.27	13.06	1.77	1.87	Kamber et al., 2005
Felsic igneous rocks	-	-	-	-	2.50	Meixner et al., 2012
Other basement rocks	-	-	-	-	1.70	Meixner et al., 2012
Granites						
DIO Wolgolla 1	77.1	5.13	22.55	3.79	3.17	This study
TEA Roseneath 1	77.7	6.41	9.08	4.76	2.67	This study
AOD Budgerygar 1	65.5	3.42	9.35	2.25	1.70	This study
LOL Stormhill 1	77.2	5.29	16.34	4.71	2.88	This study
AOP Balfour 1	64.8	1.82	8.98	2.14	1.27	This study
TEP Jandowae West 1	61.0	1.35	3.80	1.64	0.75	This study
Javel 2**	76.6	10.70	10.13	4.52	3.80	This study
PGA Bradley 1	73.0	6.87	36.46	7.18	4.87	This study
Upper Continental Crust	66.6	2.7	10.5	2.8	1.65	Rudnick&Gao, 2003
Middle Continental Crust	63.5	1.3	6.5	2.3	0.98	Rudnick&Gao, 2003
Lower Continental Crust	53.4	0.2	1.2	0.61	0.19	Rudnick&Gao, 2003
Average Continental Crust	60.6	1.3	5.6	1.81	0.87	Rudnick&Gao, 2003
Big Lake Suite	-	16.5	74	6.0	9.74	Middleton, 1979

* A density of 2.5 is used for the calculation

** Upper granite

Table 5

Well Name	Depth (m) WCR	T (°C) WCR	Depth (m) Oztemp	T (°C) Oztemp	Method
AOG Ferrett 1	1581	71	2017.78	71	DST
UOD Condamine 1	1394	49	1528.6	60.6	DST
OMN Scotia 2	2901	108	2774	100	DST
PPC Waggaba 1	766	43	Not found	Not found	DST
PPC Waggaba 1	994	43	Not found	Not found	DST
PPC Waggaba 1	1104	49	Not found	Not found	DST
PPC Waggaba 1	1152	49	Not found	Not found	DST
HEP Toobunyah 1	Not found	Not found	1219.2	97.2	Horner
SSL Clinton 1	2980	160	2804.2	146.66	DST
SSL Clinton 1	2918	154	2743.8	146.66	DST
CON Lynwood 1	2480	122	1371.6	121.67	Horner
DIO Challum 4	2352	128	2351.53	79.86	DST
SSL Juno 2	2825	149	2825.5	156.66	Horner
LEA Bodalla South 3	1715	101	1715	107.8	Horner

Figure 1

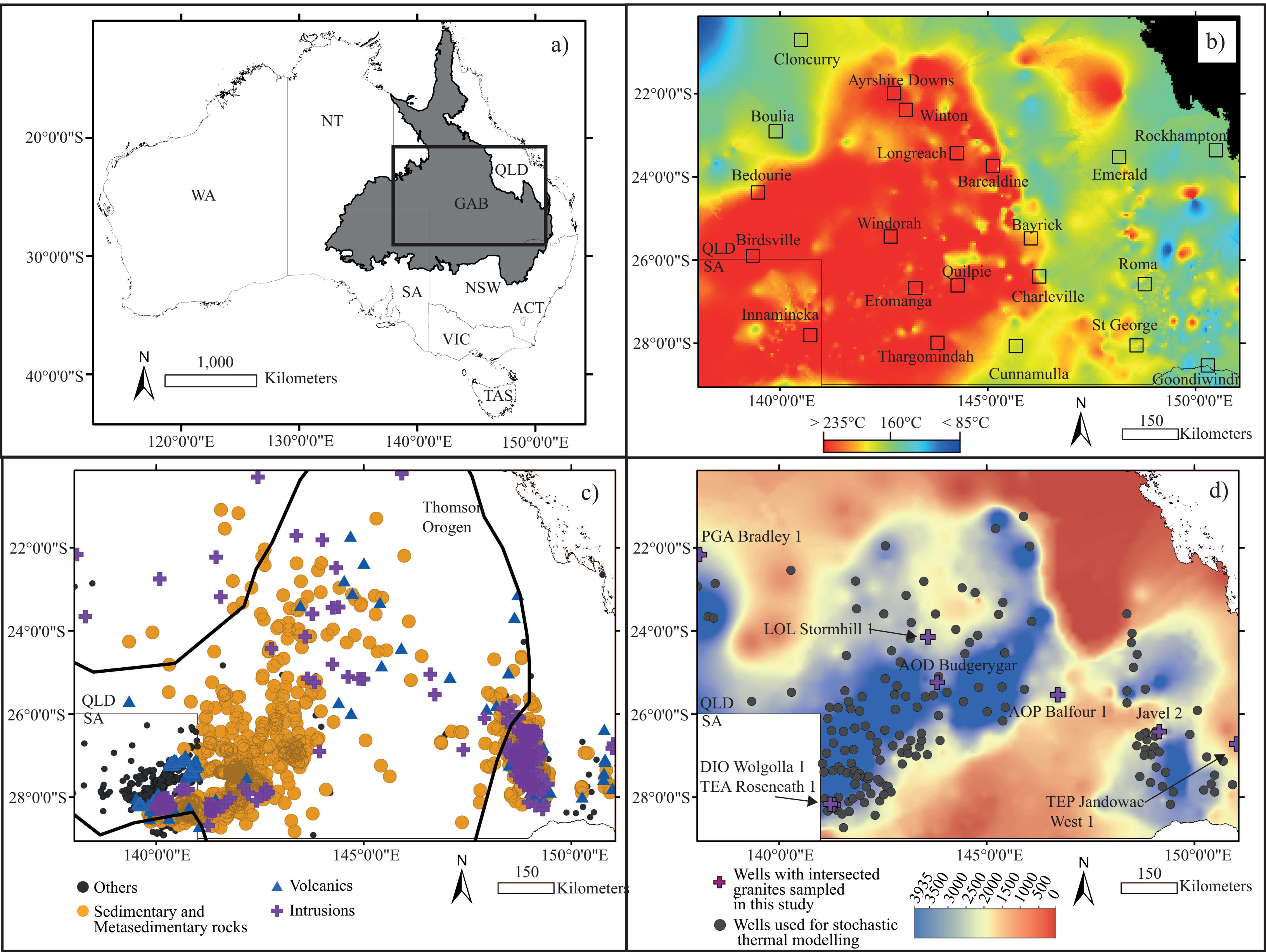

a)
NT
WA
QLD
GAB
SA
NSW
ACT
VIC
TAS
1,000
Kilometers
20°0'0"S
30°0'0"S
40°0'0"S
120°0'0"E
130°0'0"E
140°0'0"E
150°0'0"E
b)
Cloncurry
Ayrshire Downs
Winton
Boulia
Longreach
Barcaldine
Bedourie
Windorah
Birdsville
QLD
SA
Quilpie
Eromanga
Charleville
Innamincka
Thargomindah
Cunnamulla
Rockhampton
Emerald
Bayrick
Roma
St George
Goondiwindi
22°0'0"S
24°0'0"S
26°0'0"S
28°0'0"S
140°0'0"E
145°0'0"E
150°0'0"E
> 235°C
160°C
< 85°C
150
Kilometers
c)
Thomson
Orogen
QLD
SA
22°0'0"S
24°0'0"S
26°0'0"S
28°0'0"S
140°0'0"E
145°0'0"E
150°0'0"E
Others
Sedimentary and
Metasedimentary rocks
Volcanics
Intrusions
150
Kilometers
d)
PGA Bradley 1
LOL Stormhill 1
AOD Budgerygar
AOP Balfour 1
Javel 2
QLD
SA
DIO Wolgolla 1
TEA Roseneath 1
TEP Jandowae
West 1
22°0'0"S
24°0'0"S
26°0'0"S
28°0'0"S
140°0'0"E
145°0'0"E
150°0'0"E
Wells with intersected
granites sampled
in this study
Wells used for stochastic
thermal modelling
3935
3500
3000
2500
2000
1500
1000
500
0
150
Kilometers
N

Figure 2

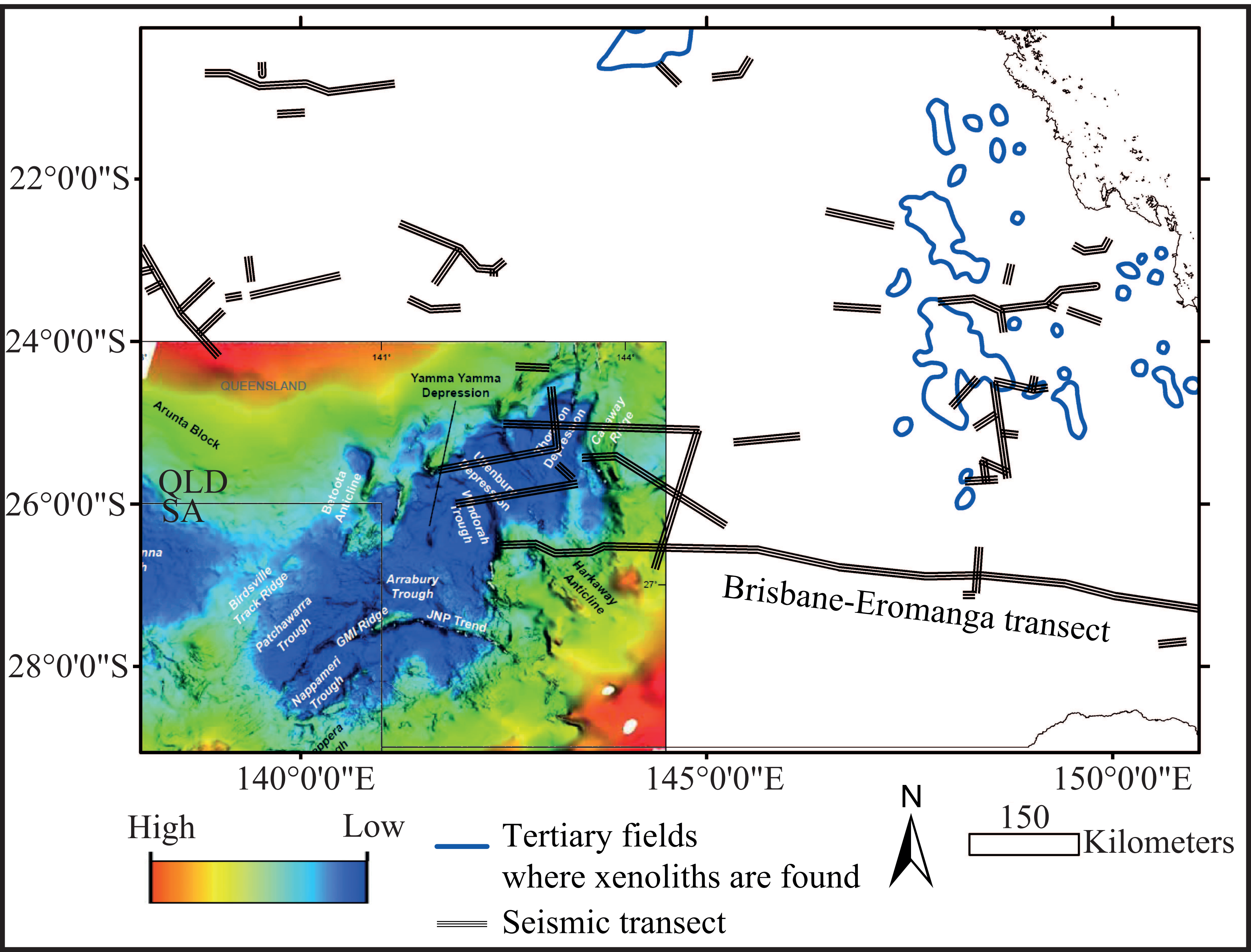

22°0'0"S
24°0'0"S
26°0'0"S
28°0'0"S
140°0'0"E
145°0'0"E
150°0'0"E
QUEENSLAND
Arunta Block
Yamma Yamma Depression
Batoota Anticline
QLD
SA
Birdsville Track Ridge
Patchawarra Trough
GMI Ridge
Nappameri Trough
Arrabury Trough
JNP Trend
Windorah Trough
Harkaway Anticline
Brisbane-Eromanga transect
High
Low
Tertiary fields where xenoliths are found
Seismic transect
N
150
Kilometers

Figure 3

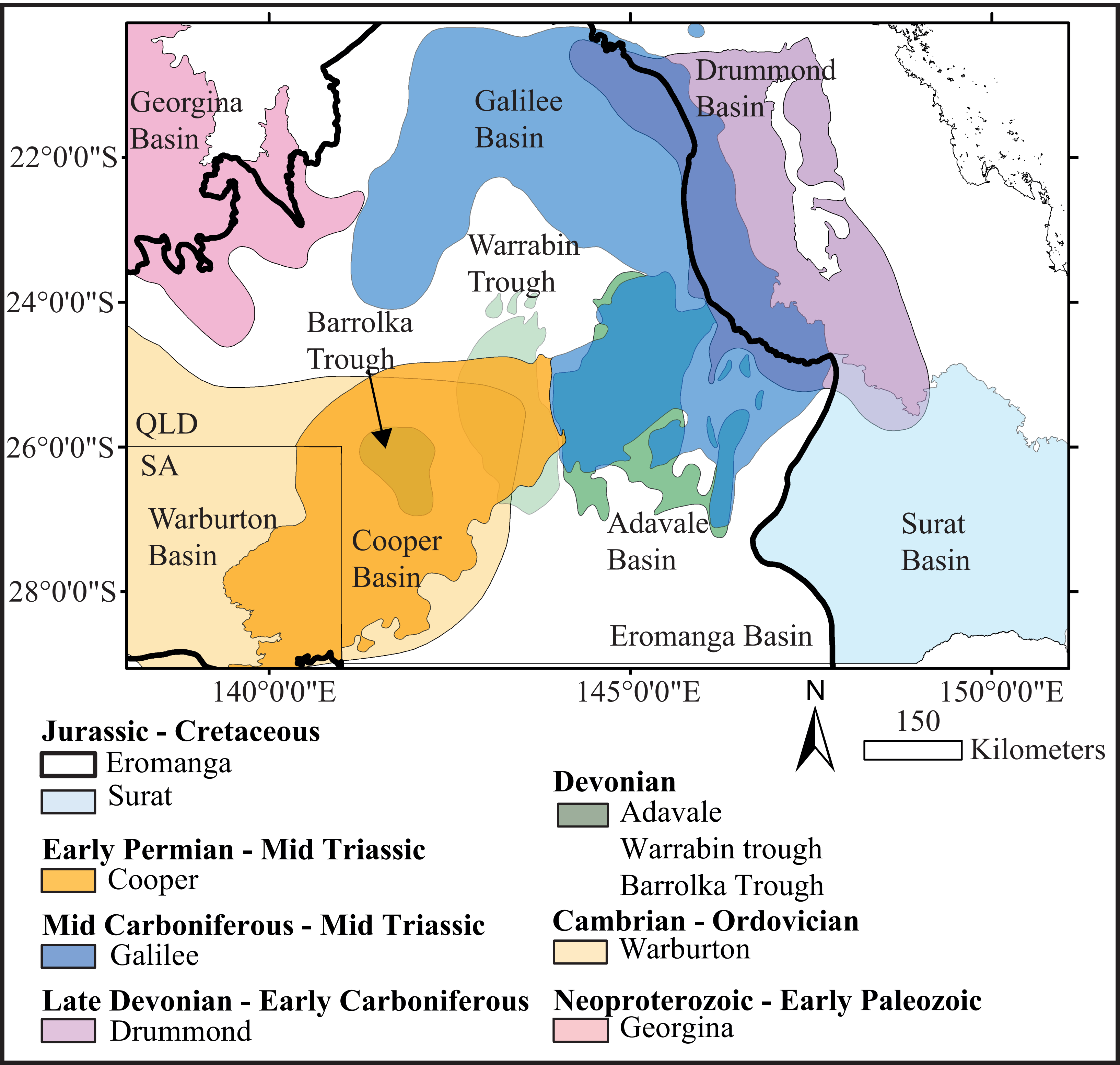
Georgina Basin
Galilee Basin
Drummond Basin
Warrabin Trough
Barrolka Trough
QLD
SA
Warburton Basin
Cooper Basin
Adavale Basin
Surat Basin
Eromanga Basin
22°0'0"S
24°0'0"S
26°0'0"S
28°0'0"S
140°0'0"E
145°0'0"E
150°0'0"E
N
150
Kilometers
Jurassic - Cretaceous
Eromanga
Surat
Early Permian - Mid Triassic
Cooper
Mid Carboniferous - Mid Triassic
Galilee
Late Devonian - Early Carboniferous
Drummond
Devonian
Adavale
Warrabin trough
Barrolka Trough
Cambrian - Ordovician
Warburton
Neoproterozoic - Early Paleozoic
Georgina

Figure 4

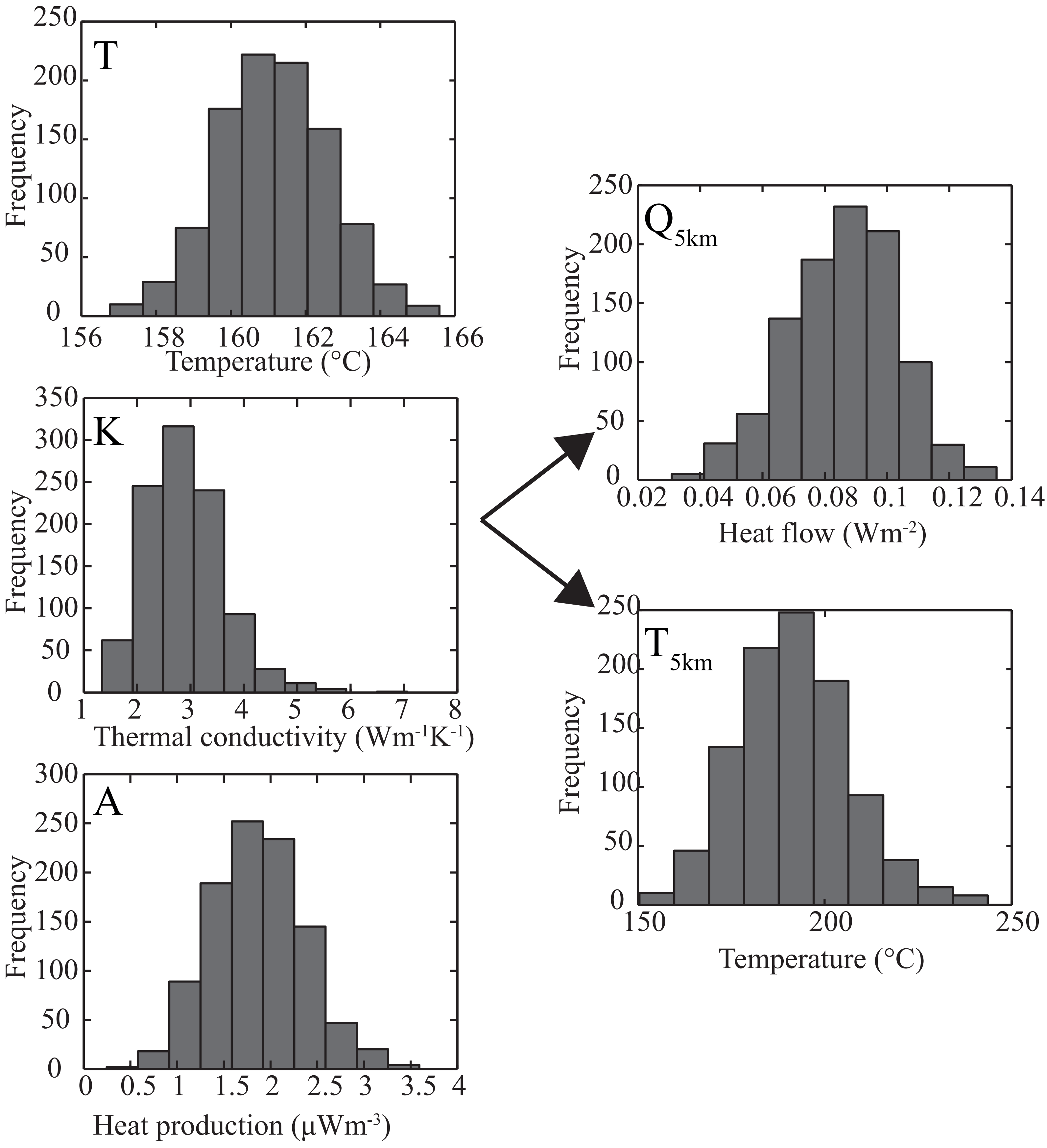
T
Frequency
Temperature (°C)
K
Frequency
Thermal conductivity (Wm-1K-1)
A
Frequency
Heat production (μWm-3)
Q5km
Frequency
Heat flow (Wm-2)
T5km
Frequency
Temperature (°C)

Figure 5

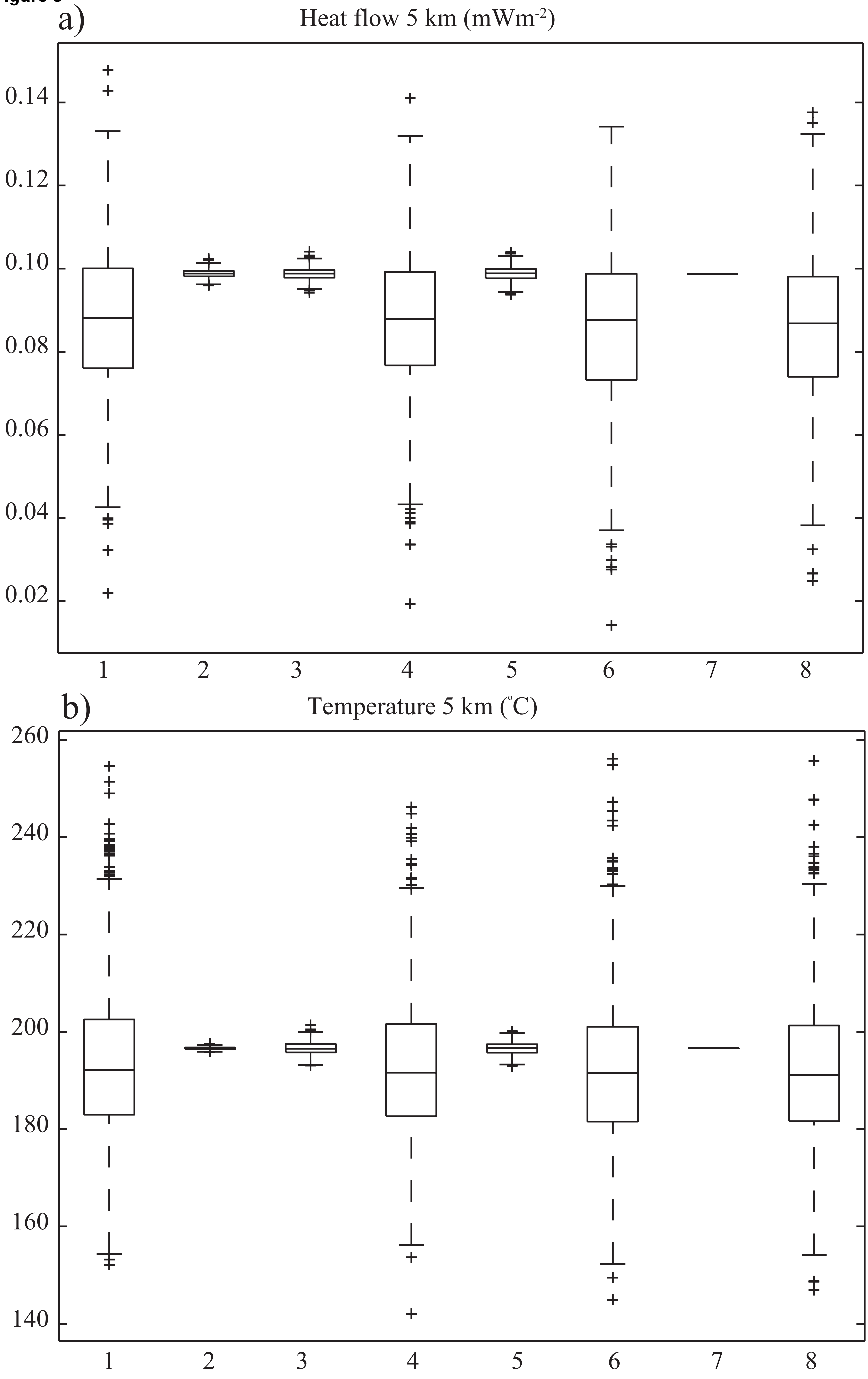

a)
Heat flow 5 km (mWm-2)
0.14
0.12
0.10
0.08
0.06
0.04
0.02
1
2
3
4
5
6
7
8
b)
Temperature 5 km (°C)
260
240
220
200
180
160
140
1
2
3
4
5
6
7
8

Figure 6

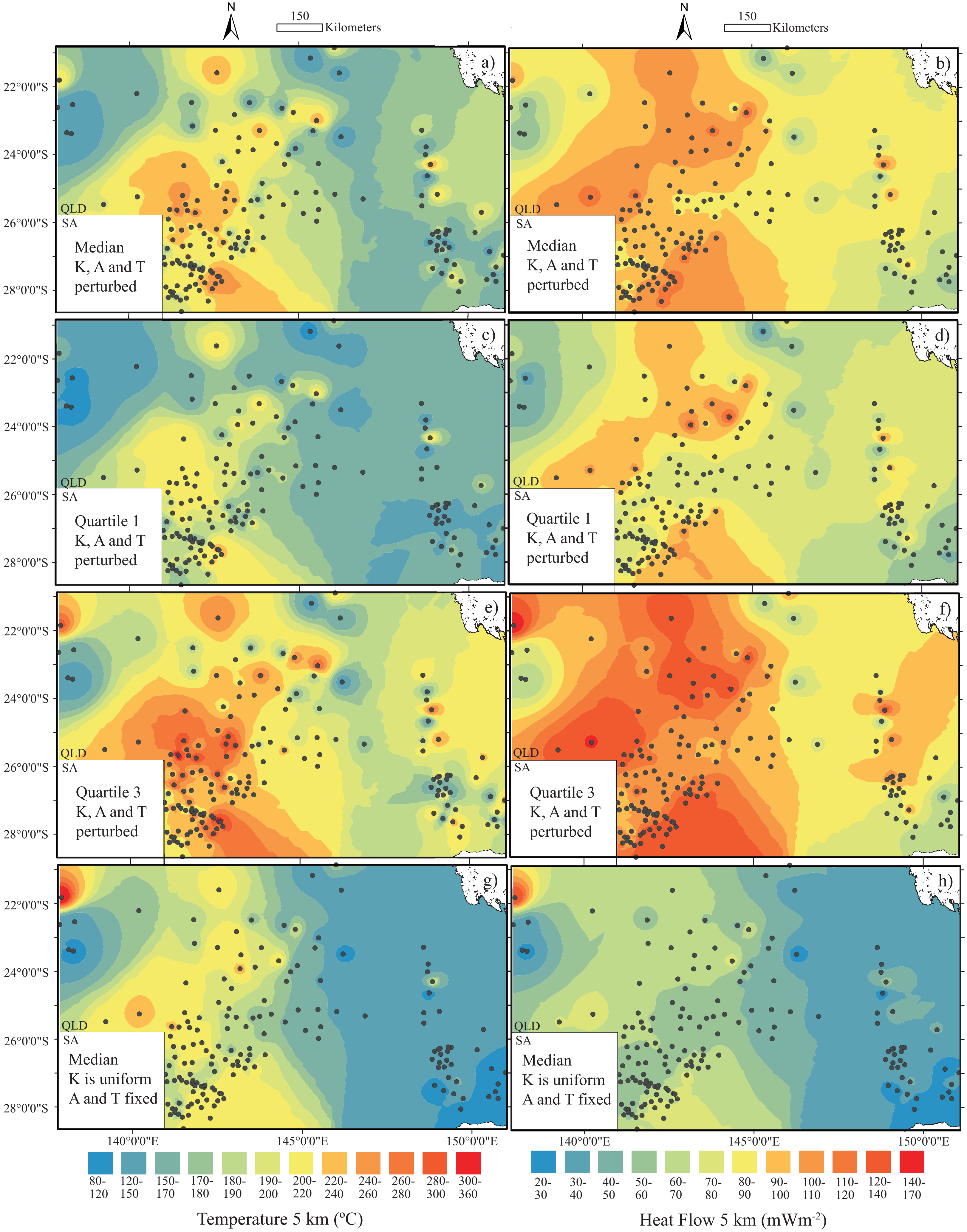
N
150 Kilometers
a)
b)
c)
d)
e)
f)
g)
h)
QLD
SA
Median K, A and T perturbed
Quartile 1 K, A and T perturbed
Quartile 3 K, A and T perturbed
Median K is uniform A and T fixed
22°0'0"S
24°0'0"S
26°0'0"S
28°0'0"S
140°0'0"E
145°0'0"E
150°0'0"E
80-120
120-150
150-170
170-180
180-190
190-200
200-220
220-240
240-260
260-280
280-300
300-360
Temperature 5 km (ºC)
20-30
30-40
40-50
50-60
60-70
70-80
80-90
90-100
100-110
110-120
120-140
140-170
Heat Flow 5 km (mWm-2)

Figure 7

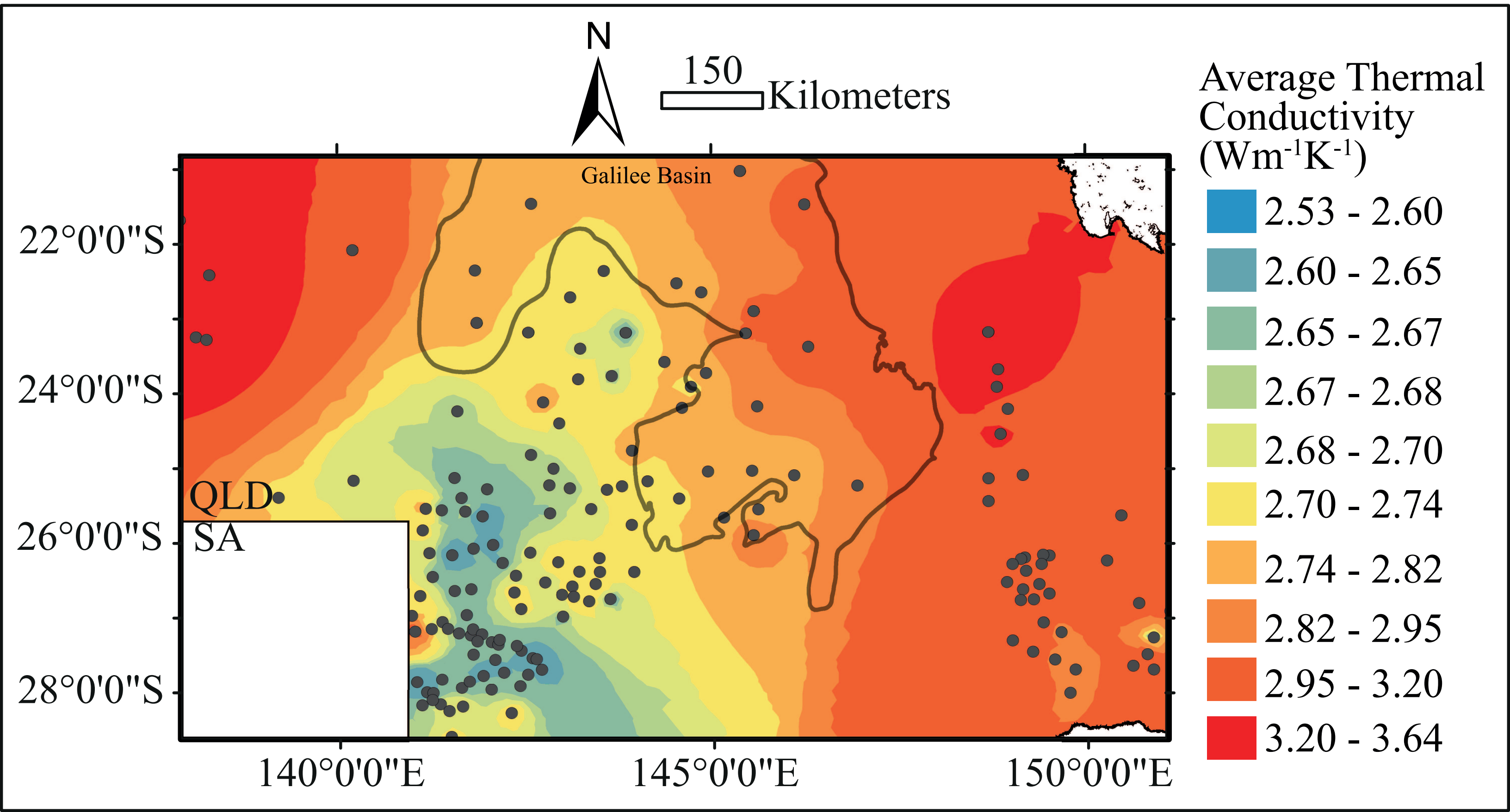

N
150
Kilometers
Average Thermal Conductivity ($Wm^{-1}K^{-1}$)
2.53 - 2.60
2.60 - 2.65
2.65 - 2.67
2.67 - 2.68
2.68 - 2.70
2.70 - 2.74
2.74 - 2.82
2.82 - 2.95
2.95 - 3.20
3.20 - 3.64
Galilee Basin
QLD
SA
22°0'0"S
24°0'0"S
26°0'0"S
28°0'0"S
140°0'0"E
145°0'0"E
150°0'0"E

Figure 8

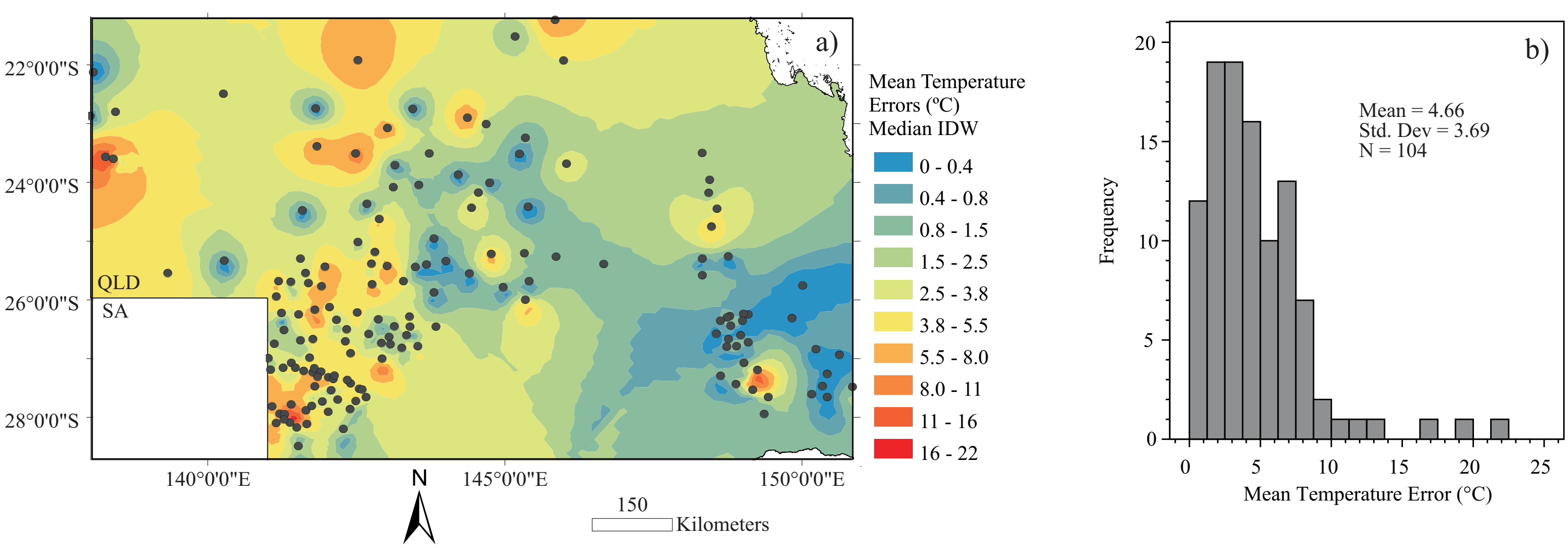
a)
22°0'0"S
24°0'0"S
26°0'0"S
28°0'0"S
140°0'0"E
145°0'0"E
150°0'0"E
QLD
SA
N
150
Kilometers
Mean Temperature Errors (ºC) Median IDW
0 - 0.4
0.4 - 0.8
0.8 - 1.5
1.5 - 2.5
2.5 - 3.8
3.8 - 5.5
5.5 - 8.0
8.0 - 11
11 - 16
16 - 22
b)
Mean = 4.66
Std. Dev = 3.69
N = 104
Frequency
Mean Temperature Error (°C)

Figure 9

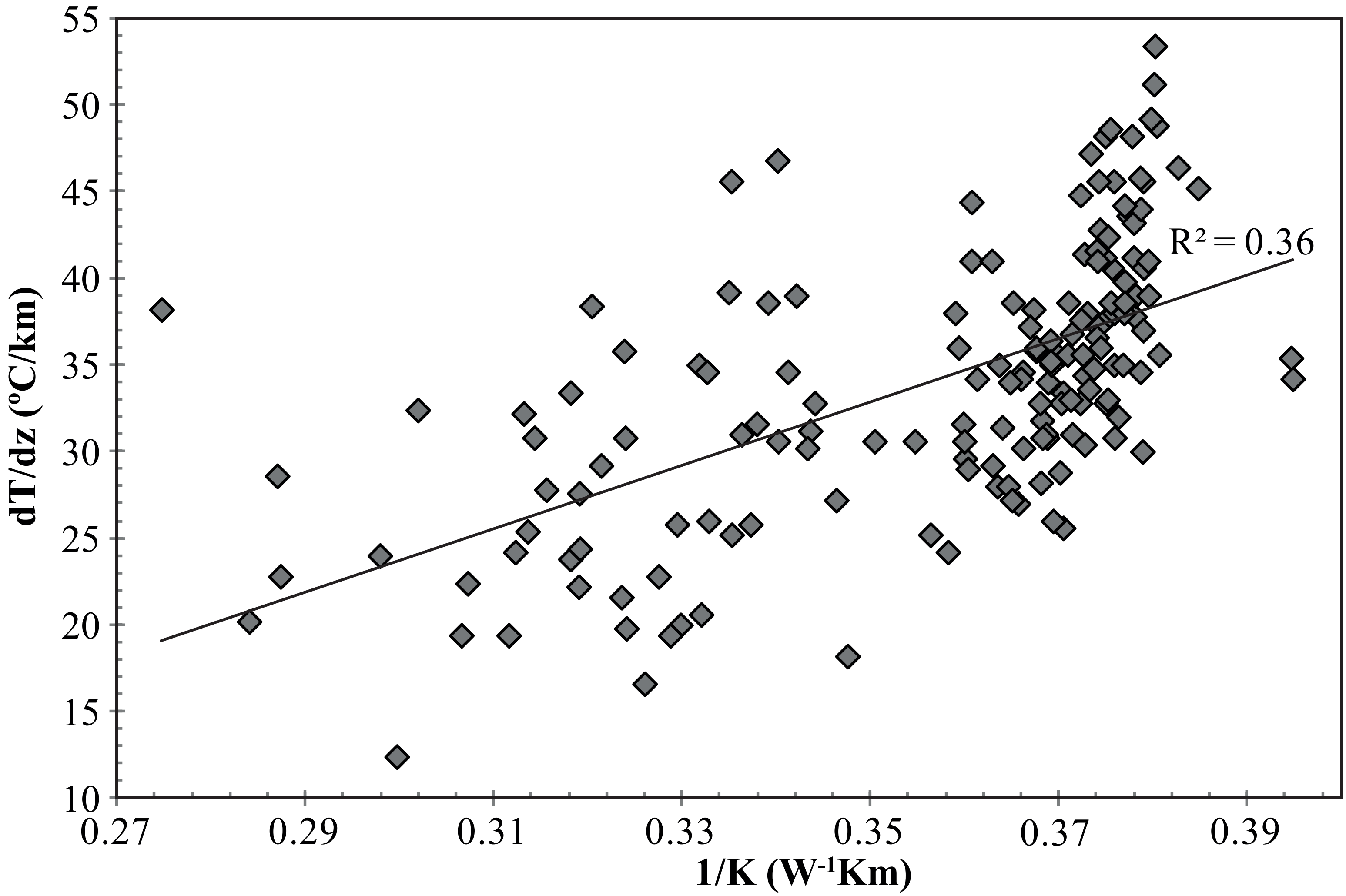

55
50
45
40
35
30
25
20
15
10
0.27
0.29
0.31
0.33
0.35
0.37
0.39
dT/dz (ºC/km)
1/K (W⁻¹Km)
R² = 0.36

Figure 10

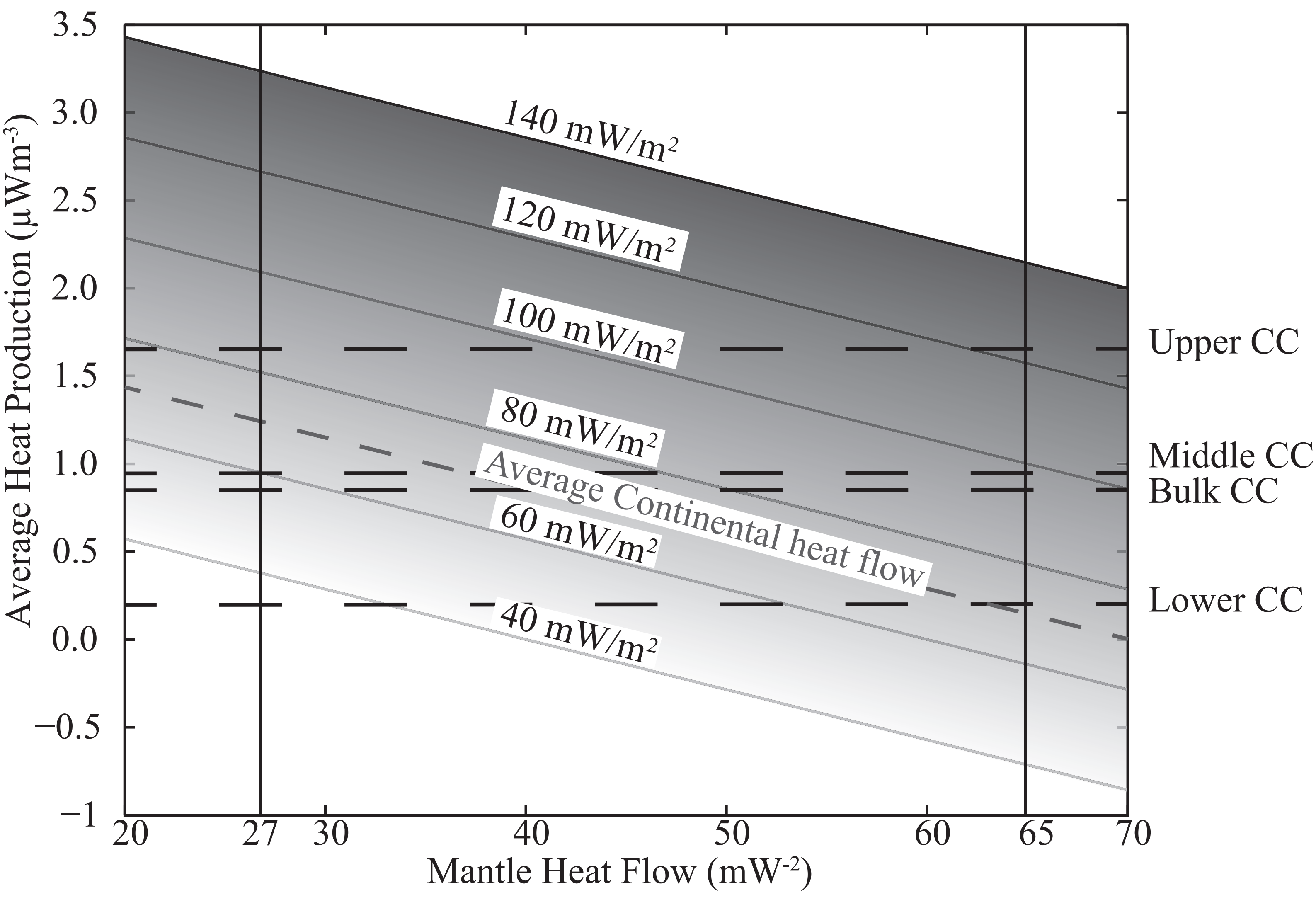

3.5
3.0
2.5
2.0
1.5
1.0
0.5
0.0
−0.5
−1
Average Heat Production (µWm-3)
140 mW/m2
120 mW/m2
100 mW/m2
80 mW/m2
Average Continental heat flow
60 mW/m2
40 mW/m2
Upper CC
Middle CC
Bulk CC
Lower CC
20
27
30
40
50
60
65
70
Mantle Heat Flow (mW-2)

Figure 11

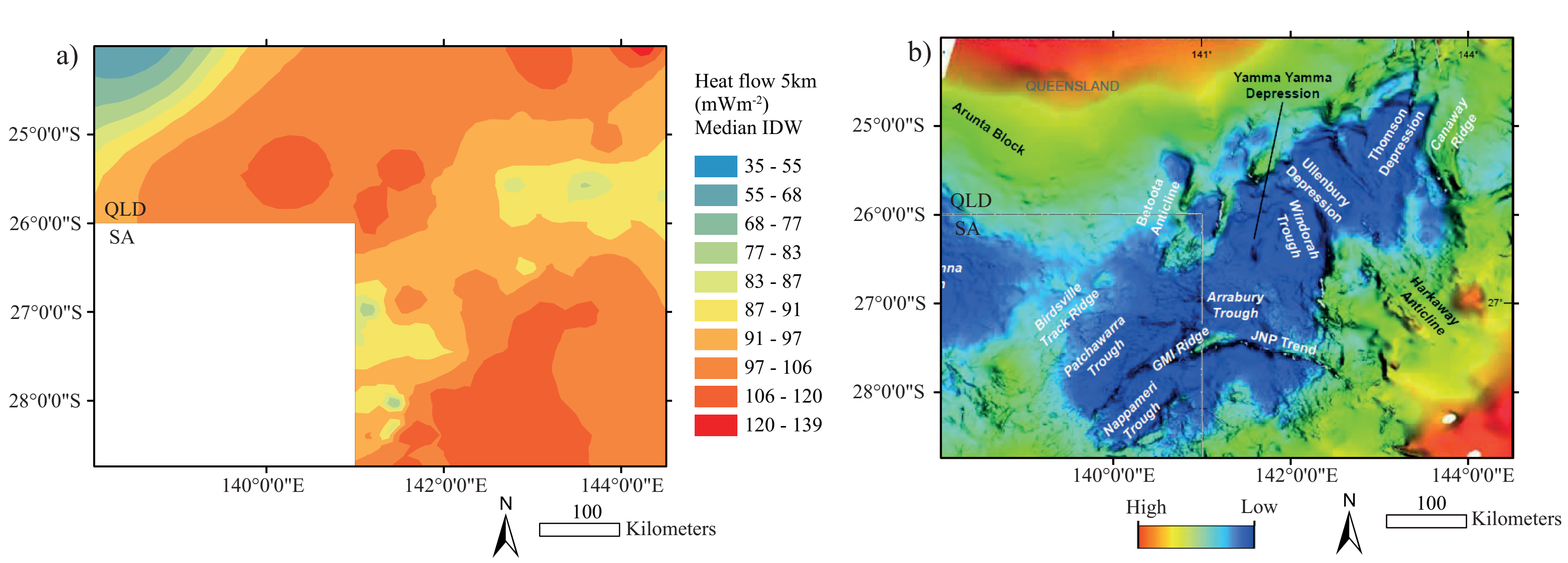
a)
Heat flow 5km
(mWm-2)
Median IDW
35 - 55
55 - 68
68 - 77
77 - 83
83 - 87
87 - 91
91 - 97
97 - 106
106 - 120
120 - 139
QLD
SA
25°0'0"S
26°0'0"S
27°0'0"S
28°0'0"S
140°0'0"E
142°0'0"E
144°0'0"E
N
100
Kilometers
b)
QUEENSLAND
Arunta Block
Yamma Yamma
Depression
Betoota
Anticline
Ullenbury
Depression
Windorah
Trough
Thomson
Depression
Canaway
Ridge
Birdsville
Track Ridge
Patchawarra
Trough
Arrabury
Trough
GMI Ridge
JNP Trend
Nappameri
Trough
Harkaway
Anticline
141°
144°
27°
QLD
SA
25°0'0"S
26°0'0"S
27°0'0"S
28°0'0"S
140°0'0"E
142°0'0"E
144°0'0"E
High
Low
N
100
Kilometers

Figure A1

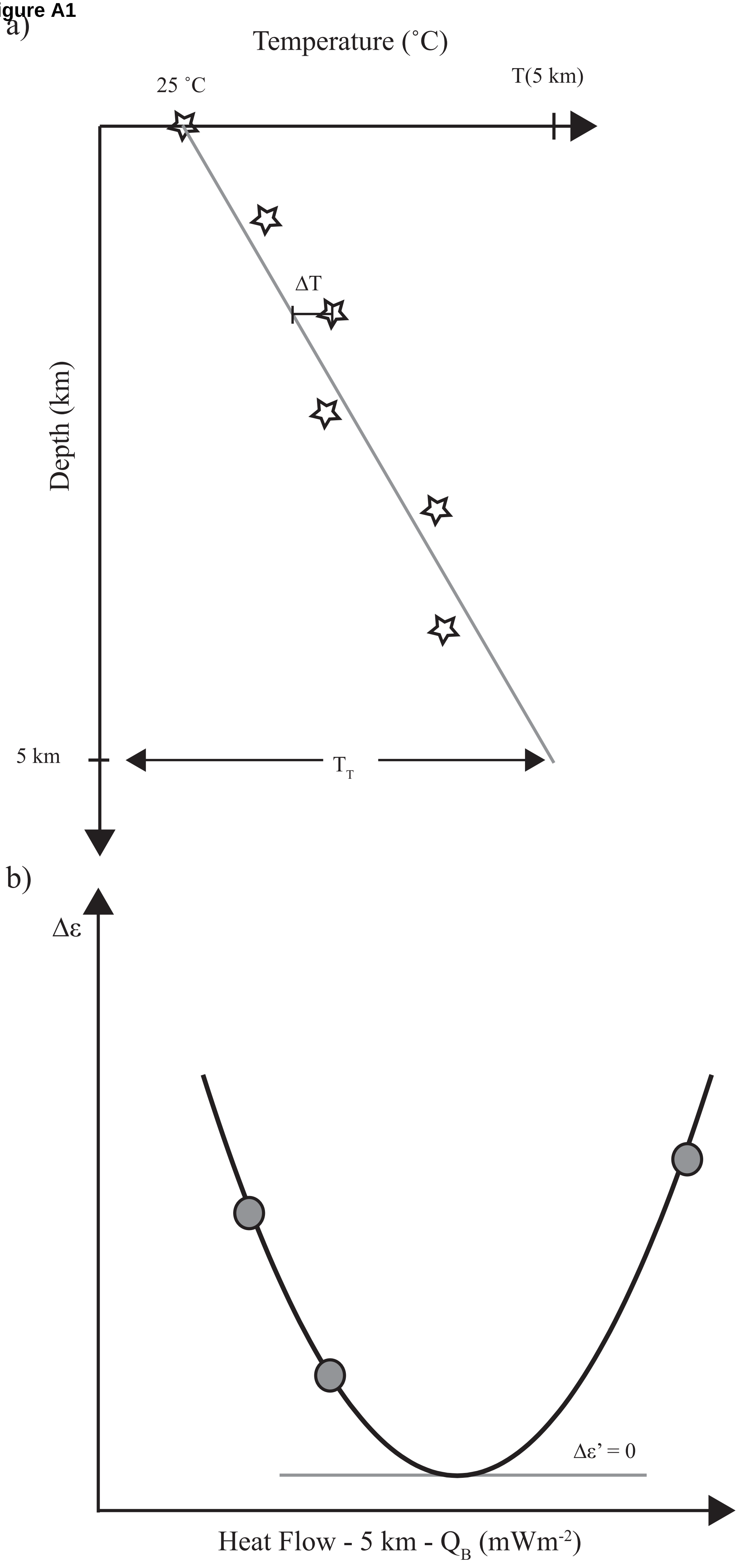

a)
Temperature (˚C)
25 ˚C
T(5 km)
ΔT
Depth (km)
5 km
T_T
b)
Δε
Δε' = 0
Heat Flow - 5 km - Q_B (mWm^{-2})

Figure captions

Figure 1: Summary of the geological features of the area of study in SW Queensland. The scale is the same for Figures 1b to 1d. a) Outline of the study area; GAB is Great Artesian Basin, WA is West Australia, SA is South Australia, QLD is Queensland, NSW is New South Wales, VIC is Victoria, NT is Northern Territory and ACT is Australian Capital territory; b) Oztemp map with towns and locations referred to in text; after Holgate and Gerner (2011); SA and QLD indicates the state border between South Australia and Queensland c) Nature of the intersected basement using data from Brown et al. (2012) for Queensland and available information from https://sarig.pir.sa.gov.au/Map for South Australia; d) Depth to basement (modified after Purdy et al., 2013) and location of new data generated in this study. Purple crosses indicate the location for new thermal conductivity and heat production values and grey points correspond to new temperature and heat flow data at 5 km depth.

Figure 2: Available information on basement structure. Image in the bottom hand left corner is the C-seismic horizon, corresponding to the top of the Early-Cretaceous Cadna-Owie formation (after Figure 5 of Radke, 2009) of the Great Artesian Basin (Cook et al., 2013). Black lines indicate the location of deep crustal seismic transects. Blue contours correspond to Tertiary intraplate volcanic fields where xenoliths were found (after O'Reilly and Griffin, 1990). Note that xenoliths are only located on the eastern side of the study area. Information on the basement structure of the study area is derived primarily from deep crustal seismic transects and seismic horizons (e.g., C-seismic horizon depicted in the bottom hand left corner image).

Figure 3: Distribution of sedimentary basins in SW Queensland that can provide thermal insulator cover to heat-producing basement rocks (Fergusson and Henderson, 2013). The thick solid line corresponds to the extent of the Eromanga Basin.

Figure 4: Schematic diagram illustrating the use of the stochastic approach. The uncertainties of three parameters: temperature (T), thermal conductivity (K) and heat production (A), have been considered to determine the uncertainties of the calculated heat flow (Q) and temperature at 5 km depth. The perturbations were performed randomly using a Gaussian distribution for temperature and heat production, and a lognormal distribution for thermal conductivity.

Figure 5: Control of input parameters (thermal conductivity, heat production and temperature) on heat flow and temperature determinations at 5 km depth. a) Range of

estimated heat flow (mWm^{-2}) at 5 km depth. b) Range of estimated temperature (ºC) at 5 km depth. Simulation 1: Temperature and heat production are fixed, thermal conductivity varies; Simulation 2: thermal conductivity and temperature are fixed, heat production varies; Simulation 3: thermal conductivity and heat production are fixed, temperature varies; Simulation 4: temperature is fixed, thermal conductivity and heat production vary; Simulation 5: Thermal conductivity is fixed, temperature and heat production vary; Simulation 6: Heat production is fixed, thermal conductivity and temperature vary; Simulation 7: Thermal conductivity, heat production and temperature are fixed; Simulation 8: Thermal conductivity, heat production and temperature vary. The widest range of uncertainties is observed when thermal conductivity data are perturbed (simulations 1, 4, 6 and 8).

Figure 6: Results of stochastic thermal modelling. a) and b), Median estimated temperature and heat flow map at 5 km depth, respectively. c) and d), First quartile (25%) estimated temperature and heat flow maps at 5 km depth, respectively. e) and f), Third quartile (75%) estimated temperature and heat flow maps at 5 km depth, respectively. g) and h), estimated temperature and heat flow maps at 5 km depth, respectively, using a uniform distribution of thermal conductivity within the interval 0.1 to 5 $Wm^{-1}K^{-1}$ and fixed heat production and temperature data. The 4 sets of maps clearly indicate a prominent SW-NE trend of lower heat flow data.

Figure 7: Average thermal conductivity (measurement unit) of the sedimentary cover. Areas of high heat flow and lower temperatures at 5 km correspond to areas with higher thermal conductivity of the sedimentary sequence (e.g. towards the Galilee Basin).

Figure 8: Reliability of the temperature and heat flow maps. a) Mean Temperature error map; b) Histogram of mean temperature errors. The majority of the wells studied have small mean temperature errors that suggest that the assumption of 1D steady-state conduction is for most cases, valid.

Figure 9: Geothermal gradient determined using temperature determination at 5 km depth versus inverse of the average thermal conductivity of the sedimentary cover. This graph illustrates the lack of correlation between sedimentary blanketing and geothermal gradient.

Figure 10: Average heat production between 5 and 40 km depth versus mantle Heat flow. Isolines correspond to heat flow at 5 km depth and dashed lines to standard crustal averages from Rudnick and Gao (2003). For areas of high heat flow (>100 mWm^{-2}), an unrealistic mantle heat flow (>65 mWm^{-2}) is required for standard crustal heat production values.

Figure 9: Geologic origin for the SW-NE trend of lower heat flow and temperatures at 5 km depth in SW Queensland. a) Close-up of median heat flow at 5 km depth as illustrated in Figure 6b with a slightly different color scale. b) The lower median heat flow SW-NE trend corresponds to basement structure and a depression indicated by the top of Cadna-Owie formation as delineated by the C seismic horizon and top of the Cadna-Owie formation (after Radke, 2009).

Figure A.1.: Schematic model to determine heat flow at 5 km depth. a) Modelled temperature profile using observed temperatures (stars) and a constant thermal conductivity. It must be noted that this temperature profile is a simple illustration and will vary with depth depending on thermal conductivity variations of the sedimentary cover. ΔT is the difference between observed and modelled temperature. T_T is the shift of the temperature profile from 0 to the best fit T_T (refer to text). b) The mean square temperature error ($\Delta\varepsilon$) is a quadratic function of heat flow at 5 km Q_T (Eq. A.11) and is used to determine the best fit T_T. The best fit Q_T corresponds to the smaller mean squared errors ($\Delta\varepsilon' = 0$), i.e., the lowest point of the quadratic function. T_T is computed using Q_T and Eq. A.9.

Table captions

Table 1: Nomenclature.

Table 2: Summary of stratigraphy encountered in the study area, listing the sedimentary formations for each basin, their stratigraphic age, approximate thickness range and estimated and measured thermal conductivities.

Table 3: Summary of analysed granites in this study, listing their location, lithological characteristics, modal mineralogy, and measured thermal conductivities.

Table 4: Key chemical characteristics and heat production values of basement granites from SW Queensland analysed in this study, and compared with other crustal materials. This table also presents heat production values for the sedimentary cover and other type of basement rocks.

Table 5: List of temperature measurement discrepancies between original data derived from well completion reports and the compiled database Oztemp from Holgate and Gerner (2011).